NATIONAL INSTITUTE OF POLAR RESEARCH

ANTARCTIC GEOLOGICAL MAP SERIES
SHEET 37 MOUNT RIISER-LARSEN

Explanatory Text of Geological Map
of
Mount Riiser-Larsen, Enderby Land, Antarctica

Masahiro ISHIKAWA, Tomokazu HOKADA, Hideo ISHIZUKA,
Hideki MIURA, Satoko SUZUKI, Masashi TAKADA and Daniel P. ZWARTZ

NATIONAL INSTITUTE OF POLAR RESEARCH
TOKYO, MARCH 2000

Antarctic Geological Map Series
Sheet 37

Mount Riiser-Larsen

Explanatory Text of Geological Map of Mount Riiser-Larsen, Enderby Land, Antarctica

Masahiro Ishikawa [1], Tomokazu Hokada [2], Hideo Ishizuka [3],
Hideki Miura [2], Satoko Suzuki [4], Masashi Takada [5] and Daniel P. Zwartz [6]

NATIONAL INSTITUTE OF POLAR RESEARCH, TOKYO, MARCH 2000

---

[1] Department of Environmental Sciences, Faculty of Education and Human Sciences, Yokohama National University, Tokiwadai, Hodogaya-ku, Yokohama 240-8501
[2] National Institute of Polar Research, 9-10, Kaga 1-chome, Itabashi-ku, Tokyo 173-8515
[3] Department of Geology, Faculty of Science, Kochi University, 5-1, Akebono-cho 2-chome, Kochi 780-8520
[4] Department of Polar Science, School of Mathematical and Physical Science, The Graduate University for Advanced Studies, 9-10, Kaga 1-chome, Itabashi-ku, Tokyo 173-8515
[5] Department of Geography, Faculty of Letters, Nara Women's University, Kita Uoya Nishi-machi, Nara 630-8506
[6] Institute for Marine and Atmospheric Research Utrecht, Utrecht University, Princetonplein 5, 3584 CC Utrecht, The Netherlands

Contents

1. Introduction

Mount Riiser-Larsen (66°45'S, 50°45'E) is located on the northern coastline of Adams Fjord along Amundsen Bay, western Enderby Land, East Antarctica (Fig. 1). Geological study of the Enderby Land started only in 1930 when Mawson's British, Australian and New Zealand Antarctic Research Expedition landed at Proclamation Island (Mawson, 1932). During the 1950s and 1960s, brief visits were made to scattered localities throughout Enderby Land by Australian Bureau of Mineral Resources geologists attached to the Australian National Antarctic Research Expeditions (Crohn, 1959; McLeod, 1959, 1964; Rucker, 1963; McLeod *et al.*, 1966). Geologists of the Soviet Antarctic Expedition undertook more extensive 1:1,000,000-scale mapping of Enderby Land in 1960s (Kamenev, 1972, 1975; Grikurov *et al.*, 1976). Australian geologists performed systematic regional studies of Enderby Land in 1974-80, where all major outcrops in Enderby Land were examined by helicopter-supported operations.

The Japanese Antarctic Research Expedition (JARE) has conducted geological surveys and investigations of the Amundsen Bay and Casey Bay areas of western Enderby Land. Of these, JARE-23, -29, -34, -36, -37, -38, -39 and -40 worked in the Mount Riiser-Larsen area, JARE-31, -39 and -40 in the Mount Pardoe and Tonagh Island areas, and JARE-34 on McIntyre Island and Hydrographer Island, and at Mount Maslen and Forefinger Point. Scientific results based on these JARE works have been published: i.e., geomorphology (Yoshida and Moriwaki, 1983; Hayashi, 1990), geology and structure (Makimoto *et al.*, 1989; Ishikawa *et al.*, 1994, Osanai *et al.*, 1999; Toyoshima

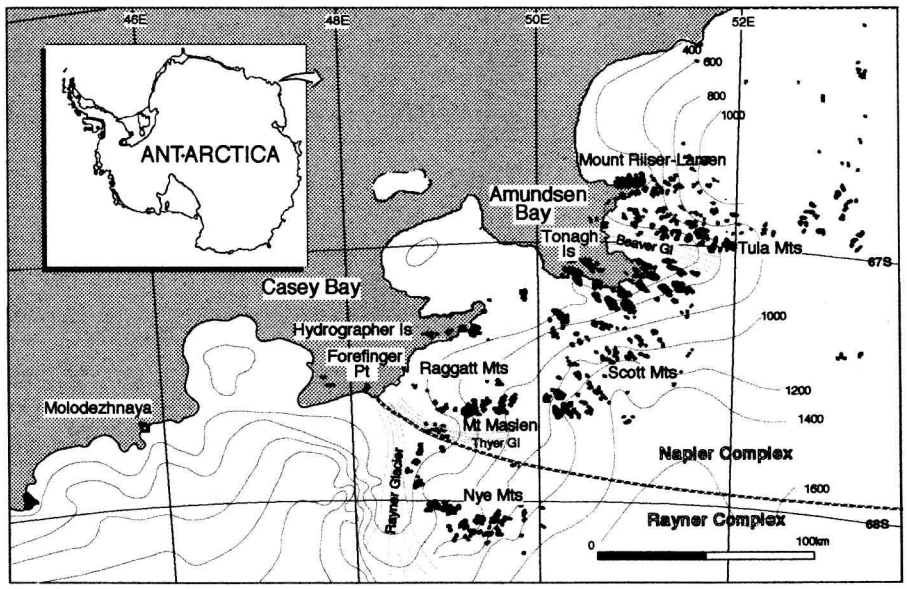

Fig. 1. Location map of the Mount Riiser-Larsen. The boundary between the Napier Complex and the Rayner Complex is after Sheraton et al. (1987).

et al., 1999), metamorphic petrology (Motoyoshi and Matsueda, 1984, 1987; Motoyoshi and Hensen, 1989; Motoyoshi *et al.*, 1990, 1994, 1995; Motoyoshi, 1996; Hokada, 1999; Hokada *et al.*, 1999; Tsunogae *et al.*, 1999), and petrochemistry and geochronology (Tainosho *et al.*, 1994, 1997; Owada *et al.*, 1994, 1999; Suzuki *et al.*, 1999; Suzuki, 2000). The geology of Mount Riiser-Larsen was studied in detail by JARE-38 for 65 days from December 16, 1996 to February 18, 1997 (Ishizuka *et al.*, 1998). Since the detailed investigation of Mount Riiser-Larsen, JARE-39 and -40 parties have carried out supplementary geological surveys of the same area. This edition of the Antarctic Geological Map Series, Sheet 37 "Mount Riiser-Larsen" (1:12,500) incorporates the field data by JARE-38 and recent laboratory work.

2. General Geology

2.1. Landforms and Cenozoic geology

The landforms of the Mount Riiser-Larsen region are mainly characterized by glacial processes. The mountain contains a serrate main ridge running about 13 km east-west with glacial cols. The south side of the ridge falls steeply into Adams Fjord, while on the north side, three large frozen lakes, Richardson Lake and the other two unnamed lakes, are contained between the ice sheet and the mountain, separated by spurs extending north from the main ridge. Bedrock crops out over most of the steep terrain on and around the ridge (Plate 1A). Higher areas around the peak are covered with a thin mantle of debris from shattered bedrocks. Extensive moraine fields and several ice-marginal moraines are developed on the lower parts of mountain flanks, especially in the western half of the region (Plate 1B). These glacial landforms suggest the glacial history of the region: past expansion and subsequent retreat, stagnation or re-advance of the ice-sheet (Yoshida and Moriwaki, 1983; Aniya, 1989; Hayashi, 1990; Miura *et al.*, 1998a, b). After the retreat of the ice sheet, glacial landforms have been locally modified by some geomorphic processes: fluvial process associated with the formation of fluvial valleys and channel landforms; marine processes for raised beaches; rock-fall processes for talus cones; periglacial processes in relation to solifluction lobes, patterned ground, frost cracks and rock glaciers on the moraine fields.

2.2. Basement geology

In northern Enderby Land of East Antarctica occurs the Napier Complex that consists mainly of metamorphic rocks with minor unmetamorphosed intrusive rocks. The metamorphic rocks are characterized by the presence of such diagnostic minerals and assemblages as sapphirine + quartz, osumilite and inverted pigeonite, indicating metamorphic temperature as high as 1000°C (*e.g.*, Sheraton *et al.*, 1987). Furthermore, the ion microprobe U-Pb dating of zircon has revealed very old age (3930 ± 10 Ma) for the tonalitic precursor of orthogneiss (Black *et al.*, 1986). The Napier Complex thus provides an excellent opportunity for understanding the nature and origin of ultra-high temperature metamorphism as well as the formative process of the Archaean continental crust.

The Mount Riiser-Larsen area is underlain by various kinds of ultra-high temperature (UHT) metamorphic rocks with subordinate amounts of unmetamorphosed intrusive rocks. The UHT basement is composed of two lithological units denoted massive gneiss unit and layered gneiss unit (Plate 1A). The massive gneiss unit is composed mainly of felsic orthogneisses and small amount of mafic granulites. The layered gneiss unit consists mainly of paragneisses with small amounts of felsic orthogneisses and mafic granulites (Plate 2A). These basement rocks are described in detail, in terms of rock associations and constituent minerals in chapter 3. Metamorphic rocks exhibit compositional layering in most kind of lithologies, on scales ranging from millimeter to tens of centimeters. Layer-parallel alignment of minerals such as sapphirine and sillimanite is also present in some paragneisses. The development of preferred orientation of metamorphic minerals is generally very weak, although elongated quartz and sillimanite define a lineation. Mafic granulites and ultramafic rocks are generally massive, although elongated orthopyroxene grains define a weak preferred orientation. Foliations are generally parallel to lithological boundaries, and dips of these foliations are gentle to moderate throughout the Mount Riiser-Larsen.

Shear zones are the most prominent structures in the area, in which the metamorphic rocks have been sheared to mylonites or sometimes pseudotachylite-like rocks. The subvertical shear zones tend to follow preexisting structures such as dike margins. The subhorizontal shear zones were developed along the preexisting lithological boundaries. The widths of shear zones mostly range from several centimeters to a few meters, but in the western part a subvertical shear zone with the width of about 300~400 m develops, striking north to south; we call this shear zone the Riiser-Larsen Main Shear Zone (RLMSZ). The RLMSZ divides the basement into two structural blocks (the main block and the western block) metamorphosed under different pressure conditions (Hokada, 1999). Indeed the dips of the foliations are discontinuous from the western to the main blocks.

3. Metamorphic Rocks

Metamorphic rocks are classified into the following rock types for mapping units, based on the modes of occurrence and lithology:

1) Garnet gneiss (Gg),
2) Garnet-sillimanite gneiss (Ggs),
3) Quartzite (Q),
4) Magnetite-quartz gneiss (Gmq),
5) Quartzo-feldspathic gneiss (Gqf),
6) Garnet-orthopyroxene quartzo-feldspathic gneiss (Ggo),
7) Sapphirine-phlogopite gneiss (Gsp),
8) Garnet felsic gneiss (Ggf),
9) Orthopyroxene felsic gneiss (Gof),
10) Mafic granulite (Gm),
11) Anorthosite (A),
12) Ultramafic rocks (U).

Chemical compositions of the representative rock types and the metamorphic minerals are listed in Tables 1 and 2, respectively. Mineral abbreviations are as follows: Ap = apatite, Bt = biotite, Cpx = clinopyroxene, Grt = garnet, Ilm = ilmenite, Meso = mesoperthite, Mnz = monazite, Mt = magnetite, Ol = olivine, Opx = orthopyroxene, Os = osumilite, Phl = phlogopite, Pl = plagioclase, Qtz = quartz, Rt = rutile, Sil = sillimanite, Spl = spinel, Spr = sapphirine, Zrn = zircon.

3.1. Garnet gneiss (Gg)

Medium- to coarse-grained garnet gneiss occurs mainly in the central part of the area, forming layers with various thicknesses, and it is commonly accompanied by garnet felsic gneiss and quartzo-feldspathic gneiss. It also sometimes accompanies a thin layer of garnet-sillimanite gneiss (Plate 2A). Major constituent minerals are garnet, quartz and feldspar (Plate 4A). The modal proportions of garnet (12-20%) and quartz (28-45%) are highly variable, giving rise to the variation of rock color (orange to pink) in the field. The garnet gneiss generally contains larger amounts of garnet than garnet felsic gneiss. The following mineral associations are observed in the garnet gneiss:

(1) garnet + quartz + mesoperthite ± plagioclase,
(2) garnet + spinel + quartz + mesoperthite ± plagioclase.

Antiperthitic plagioclase is less commonly contained in the gneiss. Quartz and feldspars commonly exhibit granoblastic texture. Garnet is commonly subhedral to anhedral in crystal form. Spinel is occasionally contained, and is generally enclosed within garnet. Zircon, rutile and ilmenite are accessories.

The garnet gneiss has the SiO_2 content ranging from 69 to 76 wt%. ACF molecular components indicate that the garnet gneiss has affinity with sedimentary rocks such as sandstone in psammitic composition. The REE concentrations of the garnet gneiss range from 100-200 times chondrite values in LREE to 20-30 times the chondrite value in HREE, showing the LREE-enriched and flat HREE patterns without the Eu anomaly.

3.2. Garnet-sillimanite gneiss (Ggs)

Garnet-sillimanite gneiss is not common rock type throughout the area, and occurs interlayered with the garnet gneiss or garnet felsic gneiss. Small blocks or pods of the garnet-sillimanite gneiss are rarely embedded in the garnet gneiss. Gray to dark gray color is typical of garnet-sillimanite gneiss. The preferred orientation of sillimanite is the most conspicuous feature.

The garnet-sillimanite gneiss comprises mainly garnet, sillimanite, quartz and feldspar minerals, of which garnet is generally coarse-grained, being up to 5 cm in diameter (Plate 2D, 4B). Other minerals such as spinel, biotite or phlogopite are also present, but less common. The following are the observed mineral associations in the garnet-sillimanite gneiss:

(1) garnet + sillimanite + quartz,
(2) garnet + sillimanite ± spinel + quartz + plagioclase,
(3) garnet + sillimanite ± spinel + quartz + mesoperthite,
(4) garnet + sillimanite + spinel + quartz + mesoperthite + plagioclase.

Garnet commonly exhibits an anhedral crystal form, while sillimanite is euhedral to subhedral. Also, sillimanite is sometimes included in garnet. Spinel is often embedded

within garnet or sillimanite. Rutile and opaque minerals are predominant accessories, but zircon and monazite are not common.

The garnet-sillimanite gneiss ranges in SiO_2 from 52 to 59 wt%, and has the highest Al_2O_3 content of 17 to 24 wt% among the samples analyzed here. There is no compositional trend diagnostic of igneous rocks. ACF molecular compositions show the garnet-sillimanite gneiss to have sedimentary features such as mudstone. The similar LREE-enriched and flat HREE patterns of the garnet gneiss are also observed in the garnet-sillimanite gneiss, although a slightly negative Eu anomaly is present in the garnet-sillimanite gneiss.

3.3. Quartzite (Q)

Medium- to coarse-grained quartzite is classified into two lithologies. One is relatively massive impure quartzite generally composed of predominant amounts of quartz, and the other is weakly foliated siliceous gneiss containing more ferromagnesian minerals than impure quartzite. Impure quartzite occurs throughout the area, interlayered mainly with garnet felsic gneiss and rarely orthopyroxene felsic gneiss and quartzo-feldspathic gneisses (Plate 2E, 3C). The layers range in thickness from several centimeters to a few meters, but mappable-scale impure quartzite is distributed on the northwestern ridge of Mount Riiser-Larsen and in the southwestern coast region. Weakly foliated siliceous gneiss occurs as pods or thin layers, commonly associated with quartzo-feldspathic gneisses (Plate 2F). It is also medium- to coarse-grained, but its lithology is heterogeneous and changes from one area to another.

The following mineral assemblages are observed in impure quartzite and siliceous gneiss:

(1) spinel + quartz ± mesoperthite ± sapphirine ± sillimanite,
(2) garnet + quartz + mesoperthite,
(3) orthopyroxene + quartz + mesoperthite,
(4) garnet + orthopyroxene + quartz + mesoperthite,
(5) sapphirine + orthopyroxene + osumilite ± sillimanite ± cordierite + quartz ± mesoperthite,
(6) spinel + sapphirine + garnet + orthopyroxene + osumilite + sillimanite + cordierite + quartz.

Assemblages (1)~(4) are observed in impure quartzite. Garnet and/or orthopyroxene-bearing assemblages (2)~(4) are generally associated with garnet-orthopyroxene quartzo-feldspathic gneiss. Relatively heterogeneous siliceous gneiss is composed of assemblages (5) and (6). Quartz is predominant, and other constituent minerals occur as inclusions in quartz or as anhedral grains distributed interstitially between quartz grains (Plate 4C). Most conspicuous, the color of quartz from impure quartz is generally pale to dark blue in hand specimens. Sapphirine and quartz are commonly in direct contact with each other, but thin cordierite and/or garnet films locally occur between sapphirine and quartz. Accessory minerals are rutile, monazite, zircon, corundum, biotite and opaque minerals. Corundum is generally associated with spinel, and is interpreted as a metastable product formed in an overstepping reaction during cooling (Motoyoshi *et al.*, 1990). Most cordierite and biotite are possibly retrograde products.

Table 1. Whole-rock chemical analyses of metamorphic rocks from Mount Riiser-Larsen.

Rock type	Gof		Gm (Qtz-free)		Gm (Qtz-bearing)		U (Phl-bearing)			U (Phl-free)			Ggf			Gg			Ggs	
Sample No.	SS0113 04	SS01210 1	SS97012 213	SS97021 303B	SS97021 310	SS97020 510	HI97011 301	HI97012 101	HI97012 102	HI97010 805	HI96123 105L	HI97010 808	SS97021 307	SS97021 201B	SS97020 505	SS97012 004	SS97021 312	SS97021 208	SS96123 003A	SS97010 505B1
SiO_2 (wt%)	70.97	69.19	47.21	49.08	50.12	51.99	40.40	45.00	49.08	45.75	46.20	51.75	68.15	72.11	74.49	68.98	72.64	75.80	52.26	58.58
TiO_2	0.30	0.45	1.07	0.86	2.67	0.65	0.08	0.10	0.25	0.07	0.15	0.15	0.33	0.12	0.29	0.53	0.52	0.36	1.59	0.96
Al_2O_3	15.19	15.48	13.58	14.15	13.18	15.19	0.98	4.30	6.38	2.48	2.87	2.93	16.26	13.79	12.75	13.20	13.15	11.85	23.03	17.42
Fe_2O_3	2.64	3.92	14.32	13.62	18.81	10.19	9.45	8.57	8.86	7.44	7.35	13.49	4.12	3.28	3.03	8.17	5.35	5.01	16.02	11.08
MnO	0.03	0.05	0.20	0.18	0.17	0.12	0.13	0.13	0.13	0.12	0.12	0.15	0.02	0.02	0.03	0.08	0.06	0.06	0.10	0.12
MgO	1.37	1.23	7.99	8.43	4.93	7.59	43.76	35.06	25.79	40.79	41.34	27.10	1.04	0.56	0.38	2.73	1.91	1.76	4.83	4.10
CaO	3.96	4.12	13.18	11.50	5.83	9.95	1.52	3.36	7.78	0.93	0.81	1.24	1.86	1.20	1.38	1.62	1.93	1.89	0.90	4.25
Na_2O	4.17	4.22	1.47	1.56	2.16	2.52	0.09	0.14	0.15	0.06	0.03	0.20	3.08	2.64	2.53	1.64	1.87	1.96	-	1.70
K_2O	1.21	1.23	0.15	0.43	0.65	0.59	0.25	1.63	0.03	-	0.04	0.17	5.00	5.02	4.33	2.38	2.72	1.64	0.10	0.52
P_2O_5	0.05	0.12	0.06	0.02	0.53	0.10	0.01	0.02	0.01	0.01	0.01	0.01	0.07	0.04	0.09	-	0.01	-	-	0.05
Total	99.89	100.02	99.23	99.83	99.04	98.88	96.67	98.30	98.46	97.64	98.92	97.19	99.93	98.78	99.29	99.33	100.16	100.34	98.82	98.79
FeO*	2.40	3.56	13.02	12.38	17.10	9.26	8.59	7.79	8.05	6.76	6.68	12.26	3.75	2.98	2.75	7.42	4.86	4.56	14.56	10.08
FeO*/MgO	1.76	2.88	1.63	1.47	3.47	1.22	0.20	0.22	0.31	0.17	0.16	0.45	3.59	5.36	7.28	2.72	2.55	2.59	3.01	2.46
(XRF)																				
Ba (ppm)	977.8	260.7	14.3	10.9	308.8	220.5	22.0	108.3	16.6	15.6	4.2	21.3	741.2	786.4	910.0	692.5	878.5	338.3	-	318.9
Co	11.2	11.5	55.9	53.2	52.9	44.4	105.4	83.6	63.4	84.6	82.9	63.9	11.0	7.1	5.5	24.0	17.0	13.2	68.5	60.8
Cr	27.2	5.2	305.6	281.5	96.1	344.4	1711	2096	2446	2118	1593	2744	15.1	8.1	12.0	166.9	100.0	98.8	804.5	202.8
Cu	6.1	1.0	65.0	76.5	129.0	58.7	-	-	1.2	-	-	12.5	0.5	6.5	3.1	49.9	21.6	18.1	11.3	55.2
Nb	3.4	12.1	4.0	2.3	24.2	12.7	1.0	0.7	2.9	1.1	3.8	1.5	17.0	10.4	27.3	29.3	12.3	7.4	36.1	14.8
Ni	55.9	18.8	147.8	140.4	88.1	136.1	2917	1975	983.1	2266	2376	1152	4.6	6.0	9.2	70.5	41.6	9.4	88.3	133.7
Rb	5.7	14.9	4.1	8.3	5.3	8.6	8.2	76.2	2.1	-	2.9	3.5	167.5	164.1	171.7	67.4	76.8	39.3	5.1	15.9
Sr	324.9	169.0	115.8	89.7	168.9	128.0	6.6	11.0	6.4	4.5	6.1	18.6	91.2	64.1	62.4	129.4	223.7	165.3	4.6	73.9
V	24.9	40.7	292.0	256.4	362.7	175.6	-	78.0	120.6	30.2	39.7	73.4	11.4	4.2	6.5	89.6	72.1	61.4	390.1	230.5
Y	3.0	17.3	23.6	21.8	44.7	18.6	3.1	7.5	12.5	3.7	10.6	16.8	127.3	155.7	155.9	53.6	31.6	29.9	72.5	56.5
Zn	33.5	64.0	94.1	102.9	148.7	86.0	48.3	70.1	71.3	41.8	41.2	106.7	25.9	24.5	30.6	62.5	44.4	33.9	143.8	37.8
Zr	154.1	231.8	43.2	37.3	111.4	41.4	8.8	14.0	34.5	13.0	23.9	18.5	325.2	225.1	236.8	208.4	193.3	137.8	322.3	217.1

Table 1. (continued)

Sample No.	SS0113 04	SS01210 1	SS97012 213	SS97021 303B	SS97021 310	SS97020 510	HI97011 301	HI97012 101	HI97012 102	HI97010 805	HI96123 105L	HI97010 808	SS97021 307	SS97021 201B	SS97020 505	SS97012 004	SS97021 312	SS97021 208	SS96123 003A	SS97010 505B1
(ICP-MASS)																				
Ga	14	19	15	15	27	17	2	6		3	3	5	31	20	23	15	19	13	37	25
Ge	0.7	0.8	1.6	1.4	1.8	1.5	0.8	1.4		0.9	1.0	<0.5	1.4	1.6	1.6	1.4	1.3	1.1	2.7	2.5
Sn	<1	1	2	2	3	2	<1	<1		2	2	<1	1	2	1	<1	<1	<1	<1	<1
La	27.9	40.0	2.87	3.53	28.0	23.7	0.82	7.65		0.72	2.17	0.71	213	143	191	29.8	46.3	39.0	2.67	53.0
Ce	34	65	8.5	9.1	52	43	1.6	23		2.7	6.8	0.9	406	255	584	49	81	67	6.3	102
Pr	2.54	5.99	1.29	1.34	6.08	4.33	0.20	2.67		0.41	0.97	0.10	40.9	26.4	42.8	4.70	7.75	6.37	1.12	11.1
Nd	8.53	23.5	7.78	7.31	26.3	17.2	0.80	9.93		1.66	4.76	0.48	151	92.4	154	16.7	27.5	23.0	9.40	42.6
Sm	1.10	4.28	2.67	2.55	6.47	3.63	0.23	1.99		0.41	1.43	0.21	31.0	19.0	29.5	3.56	4.96	3.77	5.93	9.23
Eu	1.003	1.091	0.987	0.816	1.813	0.874	0.092	0.437		0.074	0.191	0.112	1.954	1.655	1.606	1.302	1.565	1.323	0.659	2.383
Gd	0.80	3.48	3.38	3.42	6.60	3.37	0.29	1.98		0.44	1.61	0.46	24.9	20.5	25.5	4.86	4.02	3.87	7.60	10.6
Tb	0.10	0.53	0.66	0.67	1.25	0.60	0.06	0.33		0.08	0.30	0.16	4.55	3.76	4.38	1.16	0.78	0.72	1.68	1.90
Dy	0.42	2.75	4.04	4.12	7.42	3.41	0.37	1.99		0.54	1.80	1.72	23.5	23.2	25.5	8.07	4.77	4.36	11.7	12.1
Ho	0.08	0.54	0.87	0.85	1.52	0.67	0.08	0.41		0.12	0.38	0.54	4.00	5.37	5.40	1.83	1.00	0.92	2.83	2.72
Er	0.21	1.51	2.50	2.37	4.45	1.87	0.22	1.20		0.39	0.98	2.03	10.4	16.9	16.5	5.28	3.14	2.78	7.87	7.72
Tm	0.024	0.211	0.407	0.359	0.654	0.285	0.037	0.177		0.063	0.152	0.354	1.451	2.984	2.544	0.838	0.470	0.412	1.298	1.242
Yb	0.18	1.20	2.46	2.29	4.05	1.67	0.21	1.11		0.44	0.80	2.42	7.98	18.4	14.5	4.74	3.00	2.58	7.80	7.09
Lu	0.036	0.167	0.353	0.328	0.609	0.240	0.034	0.162		0.070	0.111	0.403	1.115	2.853	2.072	0.699	0.446	0.388	1.164	1.022
Hf	3.3	5.0	1.1	0.9	3.1	1.0	0.2	0.9		0.4	0.8	0.7	12	8.6	9.4	5.8	5.1	3.1	8.9	7.2
Ta	<0.1	0.5	0.1	0.2	1.1	0.8	<0.1	0.2		<0.1	0.2	<0.1	0.5	0.4	1.2	3.2	0.7	0.8	2.6	2.4
Pb	17	20	<5	<5	9	12	<5	<5		<5	<5	<5	104	52	30	13	40	28	<5	8
Th	0.66	2.42	0.06	<0.05	5.73	3.48	0.37	3.63		0.06	0.50	0.15	147	68.3	200	4.34	13.5	2.16	1.44	6.25
U	0.22	1.40	<0.05	<0.05	0.73	0.42	0.16	0.33		<0.05	0.14	<0.05	6.94	12.2	15.9	0.87	0.67	0.34	0.41	0.90

All analytical data are after Suzuki (2000).

Table 2. Representative electron microprobe analyses of constituent minerals.

Mineral	Spr	Spr	Spr	Opx	Opx	Opx	Grt	Grt	Grt	Os	Os	Spl	Spl
Sample No.	TH970- 21326	TH970- 20713	TH970- 10820	TH970- 20713	R9802- 2301A	SS970- 12401	TH970- 10516	R9802- 2301A	SS970- 21307	TH970- 21326	TH970- 11709	TH970- 21321	TH970- 11709
Rock type	Q	Gq	Gsp	Gq	Ggo	Gof	Gg	Ggo	Ggf	Q	Gq	Ggs	Gq
SiO_2 (wt%)	14.33	14.33	14.23	48.74	50.66	51.40	38.95	38.82	39.89	62.59	62.31	0.17	0.00
TiO_2	0.08	0.05	0.02	0.46	0.21	0.05	0.00	0.00	0.09	0.02	0.06	0.01	0.00
Al_2O_3	60.86	60.95	62.99	11.90	5.49	1.20	22.03	22.25	22.36	23.68	23.26	58.15	63.46
Cr_2O_3	0.02	0.13	0.05	0.00	0.00	0.00	0.02	0.06	0.00	0.00	0.00	4.93	0.00
FeO*	7.23	8.75	2.77	15.49	22.49	26.23	26.85	28.10	27.77	1.41	2.25	21.34	22.63
MnO	0.00	0.01	0.01	0.10	0.09	0.82	0.32	0.25	0.22	0.04	0.00	0.00	0.00
ZnO	0.00	0.00	0.08	0.01	0.03	-	-	0.06	0.00	0.07	0.00	6.00	0.90
MgO	17.28	16.22	19.43	24.15	21.17	20.04	9.83	9.22	8.77	8.15	7.65	9.61	12.69
CaO	0.00	0.00	0.01	0.04	0.13	0.40	1.48	1.62	1.66	0.00	0.01	0.02	0.00
Na_2O	0.00	0.02	0.00	0.03	0.01	0.02	0.00	0.01	0.01	0.35	0.34	-	0.07
K_2O	0.00	0.00	0.00	0.00	0.00	0.00	0.00	0.00	0.00	4.16	4.51	0.00	0.00
Total	99.80	100.46	99.59	100.92	100.28	100.16	99.48	100.39	100.77	100.47	100.39	100.23	99.75
cations	O=20			O=6			O=12			O=30		O=4	
Si	1.704	1.704	1.662	1.737	1.877	1.953	2.999	2.981	3.035	10.234	10.252	0.005	0.000
Ti	0.007	0.004	0.002	0.012	0.006	0.001	0.000	0.000	0.005	0.002	0.007	0.000	0.000
Al	8.529	8.543	8.668	0.500	0.240	0.054	1.999	2.013	2.005	4.563	4.510	1.883	1.984
Cr	0.002	0.012	0.005	0.000	0.000	0.000	0.001	0.004	0.000	0.000	0.000	0.107	0.000
Fe	0.719	0.870	0.270	0.462	0.697	0.833	1.729	1.804	1.767	0.193	0.310	0.490	0.502
Mn	0.000	0.001	0.001	0.003	0.003	0.026	0.021	0.016	0.014	0.006	0.000	0.000	0.000
Zn	0.000	0.000	0.007	0.000	0.001	-	-	0.003	0.000	0.008	0.000	0.122	0.018
Mg	3.064	2.876	3.382	1.283	1.169	1.135	1.129	1.055	0.995	1.987	1.876	0.394	0.502
Ca	0.000	0.000	0.001	0.002	0.005	0.016	0.122	0.133	0.135	0.000	0.002	0.001	0.000
Na	0.000	0.005	0.000	0.002	0.001	0.001	0.000	0.001	0.001	0.111	0.108	-	0.004
K	0.000	0.000	0.000	0.000	0.000	0.000	0.000	0.000	0.000	0.867	0.947	0.000	0.000
Total	14.025	14.015	13.998	4.001	3.999	4.019	8.000	8.010	7.957	17.971	18.012	3.002	3.010
X_{Mg}	0.81	0.77	0.93	0.74	0.63	0.58	0.40	0.37	0.36	0.91	0.86	0.45	0.50
almandine							0.58	0.60	0.61				
pyrope							0.38	0.35	0.34				
grossular							0.04	0.04	0.05				
spessartine							0.01	0.01	0.01				

* total Fe as FeO

Sample No.	Rock name
TH97021326	Sapphirine-orthopyroxene-osumilite-bearing siliceous gneiss (Q)
TH97020713	Sapphirine-orthopyroxene-bearing quartzo-feldspathic gneiss (Gq)
TH97010830	Sapphirine-phlogopite gneiss (Gsp)
R98022301A	Garnet-orthopyroxene-bearing quartzo-feldspathic gneiss (Ggo)
SS97012401	Orthopyroxene felsic gneiss (Gof)
TH97010516	Spinel-bearing garnet gneiss (Gg)
SS97021307	Garnet felsic gneiss (Ggf)
TH97011709	Garnet-osumilite-bearing quartzo-feldspathic gneiss (Gq)
TH97021321	Spinel-bearing Garnet-sillimanite gneiss (Ggs)

All analytical data are after Hokada (1999).

3.4. Magnetite-quartz gneiss (Gmq)

Magnetite-quartz gneiss, having black to dark-green color, is widespread in the area, occurring as layers and sometimes blocks within the garnet felsic gneiss and rarely orthopyroxene felsic gneiss. The thickness of these layers ranges from several centimeters to several tens of centimeters, but it is rarely more than a few meters. Also, the magnetite-quartz gneiss occurs as thin layers between the layers of the garnet-sillimanite gneiss, indicating that the magnetite-quartz gneiss is sedimentary in origin (banded iron formation).

Medium- to sometimes coarse-grained quartz and magnetite are the main constituent minerals, sometimes combined with clinopyroxene, orthopyroxene and/or garnet (Plate 3A). Of these, pyroxenes, if they are free of secondary alteration or shearing effect, show two modes of occurrence, depending on the difference in whole-rock composition. In iron-rich rocks, clinopyroxene and orthopyroxene exhibit intimate exsolution intergrowth, which consists of blebby and/or lamellae exsolution of clinopyroxene in the orthopyroxene host (Plate 4D). Of these, clinopyroxene lamellae are generally broad, up to 0.3 mm across on a plane close to (001) in orthopyroxene, but fine lamellae (< 0.02 mm) also occur. These exsolution textures strongly suggest the existence of pigeonite, now inverted, during the peak metamorphic stage. In magnesian rocks, both orthopyroxene and clinopyroxene occur only as discrete grains with no intergrowth texture.

3.5. Quartzo-feldspathic gneiss (Gqf)

Medium-grained quartzo-feldspathic gneiss occurs as layers of meters to several tens meters in thickness, and shows a white-colored appearance in the field. It commonly demonstrates internal compositional layering, and its lithology varies. It consists of mainly quartz and feldspar, either mesoperthite or plagioclase. The principal mafic mineral is commonly garnet, sometimes accompanied by osumilite and/or sapphirine. A relatively massive portion composed of garnet + quartz + feldspar resembles garnet felsic gneiss (Plate 2E). Garnet-free and sapphirine-orthopyroxene-bearing quartzo-feldspathic gneiss is also present (Plate 3B). The following mineral assemblages are observed in quartzo-feldspathic gneisses:

(1) garnet + quartz + mesoperthite,
(2) garnet + osumilite ± sillimanite ± orthopyroxene + quartz + mesoperthite,
(3) garnet + osumilite + orthopyroxene + spinel + sapphirine + quartz + mesoperthite,
(4) sapphirine + orthopyroxene ± osumilite ± sillimanite + quartz + plagioclase.

The assemblage (1) is the most abundant mineral assemblage. Other assemblages generally occur interlayered with the assemblage (1). Garnet-osumilite-bearing assemblages (2) and (3) are restricted to the central part of the area. Garnet-free and plagioclase-bearing sapphirine + orthopyroxene + quartz + plagioclase assemblage (4) are also locally present. In the western block, assemblage (4) is dominant. Sapphirine exhibits an anhedral crystal form, and is generally in direct contact with quartz (Plate 4E). In some cases, orthopyroxene + sillimanite films occur between sapphirine and quartz. Osumilite in quartzo-feldspathic gneiss is euhedral to subhedral, and is commonly replaced by fine-grained symplectite of cordierite + K-feldspar + quartz + orthopyroxene. Euhedral sillimanite is locally contained, and is generally associated with or surrounded

by quartz. In all assemblages, rutile, monazite, zircon, biotite and opaque minerals are accessories. Most biotite is a possibly retrograde product.

3.6. Garnet-orthopyroxene quartzo-feldspathic gneiss (Ggo)

Medium- to coarse-grained garnet-orthopyroxene quartzo-feldspathic gneiss occurs commonly accompanied by garnet and/or orthopyroxene-bearing impure quartzite, sapphirine and osumilite-bearing siliceous or aluminous layers (Plate 3C, 4F). It is quite heterogeneous in appearance and irregular-shaped patches or veins composed some of garnet, orthopyroxene, quartz or feldspar are developed. Garnet megacrysts of up to 10 cm and euhedral sapphirine porphyroblasts are observed in some portions.

The following mineral assemblages are observed in garnet-orthopyroxene quartzo-feldspathic gneiss, and in associated impure quartzite or aluminous layers:

(1) garnet + orthopyroxene + plagioclase + quartz,
(2) garnet + orthopyroxene + mesoperthite + quartz,
(3) garnet + quartz + mesoperthite,
(4) orthopyroxene + quartz + mesoperthite,
(5) spinel + sapphirine + garnet + orthopyroxene + osumilite + sillimanite + quartz + cordierite,
(6) sapphirine + garnet ± spinel ± orthopyroxene + quartz ± mesoperthite,
(7) sapphirine + orthopyroxene ± osumilite ± sillimanite + quartz ± plagioclase ± mesoperthite,
(8) spinel + sapphirine + orthopyroxene + K-feldspar,
(9) sapphirine + orthopyroxene + K-feldspar + osumilite.

The assemblages (1)~(2) are the abundant mineral assemblages. Plagioclase is generally antiperthite. In the coarse-grained rock, quartz is commonly bluish in color, and plagioclase and mesoperthite are white. Garnet is anhedral or rounded. Orthopyroxene is subhedral and granoblastic in texture. Orthopyroxene-free (3) and garnet-free (4) assemblages are also locally observed. Sapphirine-bearing aluminous layer in garnet-orthopyroxene quartzo-feldspathic gneiss is composed of mineral assemblages (6)~(9). Osumilite is commonly replaced by fine-grained symplectite of cordierite + K-feldspar + quartz + orthopyroxene (Plate 5A). Rutile, monazite, zircon, biotite, cordierite and opaque minerals are accessories. Most biotite and cordierite are possibly retrograde products.

3.7. Sapphirine-phlogopite gneiss (Gsp)

Sapphirine-phlogopite gneiss exists sporadically in the area (Plate 3D). It occurs as lenses or blocks of several tens of centimeters to a few meters in thickness, enclosed within felsic gneiss, quartzo-feldspathic gneiss or mafic granulite. Idiomorphic sapphirine porphyroblast is conspicuous. Phlogopite and plagioclase (rarely K-feldspar) with or without orthopyroxene constitute the matrix of the gneiss. Garnet is rarely formed as porphyroblasts surrounding sapphirine. This lithology does not occur on a mappable scale, but its distribution is emphasized on the geological map.

The following mineral assemblages are observed in sapphirine-phlogopite gneiss under a microscope:

(1) sapphirine + phlogopite + plagioclase,
(2) sapphirine + phlogopite + orthopyroxene ± cordierite + plagioclase,

(3) sapphirine + phlogopite + orthopyroxene + cordierite ± spinel ± sillimanite + K-feldspar.

Phlogopite is the dominant mineral. Sapphirine commonly occurs as idiomorphic porphyroblasts of up to several centimeters order. Other minerals such as orthopyroxene, cordierite, sillimanite, spinel, plagioclase and mesoperthite are subordinated. Quartz is not present. Corundum rarely occurs, and is generally associated with spinel or sapphirine.

3.8. Garnet felsic gneiss (Ggf)

Garnet felsic gneiss occurs mainly in the central to northwestern part of the main block, commonly accompanied by orthopyroxene felsic gneiss, garnet gneiss, quartzo-feldspathic gneiss, garnet-sillimanite gneiss, mafic granulite, impure quartzite and magnetite-quartz gneiss (Plate 2A), but in the southern to southwestern part several layers of the garnet felsic gneiss are present, only within the orthopyroxene felsic gneiss. The modal proportions of garnet (2-10%) and quartz (25-40%) are highly variable, giving rise to the variation of rock-color (grayish pink to white) (Plate 2B, C). The mineral assemblage of garnet felsic gneiss is similar to that of garnet gneiss, but the garnet felsic gneiss generally contains smaller amounts of garnet than the garnet gneiss (Plate 5B).

The garnet felsic gneiss commonly exhibits granoblastic texture, and ranges from medium to coarse in grain size. Major constituent minerals include garnet, quartz and feldspar minerals, of which garnet is commonly subhedral to anhedral in crystal form. Mesoperthite is the common feldspar in the garnet felsic gneiss, but plagioclase is less commonly contained. Zircon, apatite, rutile, monazite and ilmenite are accessories.

The SiO_2 content of the garnet felsic gneiss ranges from 68 to 78 wt%. CIPW normative compositions indicate the garnet felsic gneiss to be classified into granite. The REE patterns of the garnet felsic gneiss are relatively flat in HREE and enriched in LREE, and display the negative Eu anomaly. The garnet felsic gneiss characteristically contains high content of incompatible elements as well as REEs. This may be attributed to relatively high abundance of accessory minerals such as monazite, zircon, apatite, and the small REE-enriched inclusions in garnet.

3.9. Orthopyroxene felsic gneiss (Gof)

Orthopyroxene felsic gneiss is widespread in the area. In the central to western part of the main block, it is commonly interlayered with garnet felsic gneiss, garnet gneiss, quartzo-feldspathic gneiss, mafic granulite and rarely garnet-sillimanite gneiss, impure quartzite and magnetite-quartz gneiss. The layers of the orthopyroxene felsic gneiss range from several tens of centimeters to a few tens of meters in thickness. In the southern to eastern part, the orthopyroxene felsic gneiss is also predominant (massive gneiss unit), but the layering structure is not conspicuous and the lithology is rather monotonous. It is occasionary includes patches or thin layers of mafic to ultramafic rocks (Plate 3E, F). Compositional layering sometimes develops weakly in the orthopyroxene felsic gneiss.

The orthopyroxene felsic gneiss is pale purple to gray in color and medium to coarse in grain size, and commonly exhibits granoblastic texture. Most commonly, it is massive but locally foliated. Pleochroic orthopyroxene, quartz and feldspar minerals are the main constituents (Plate 5C); the first two minerals display euhedral to subhedral

crystal form. Quartz is often elongated as defining a mineral lineation. Orthopyroxene is sometimes altered to biotite along cleavages and margins. Feldspar minerals include antiperthitic plagioclase and mesoperthite, commonly forming perthite to mesoperthite. A quartz + feldspar association without orthopyroxene also develops, forming thin layers several centimeters to a few meters thick. Accessory minerals include zircon, monazite, apatite, ilmenite, magnetite, and rarely rutile, titanite and allanite.

Whole-rock analyses of the orthopyroxene felsic gneiss show SiO_2 content from 64 to 73 wt%. The orthopyroxene felsic gneiss is plotted in the non-alkaline field on the alkali-silica diagram, and has a calc-alkaline affinity on the AFM diagram. Also, CIPW normative compositions indicate the orthopyroxene felsic gneiss to be classified into tonalite to granodiorite. As compared with other acidic rocks, the orthopyroxene felsic gneiss is lower in Fe_2O_3, MgO, MnO, TiO_2, Rb and K_2O/Na_2O ratios, and higher in Sr. The orthopyroxene felsic gneiss has a wide range of REE concentrations from 10-100 times chondrite values in LREE to 0.2-20 times chondrite values in HREE, which seems to be antithetically related to the SiO_2 content, namely, the REE concentrations decrease with increasing SiO_2 content. These geochemical features suggest that the orthopyroxene felsic gneisses are similar to TTG (tonalite-trondhjemite-granodiorite) of the Archaean terrane elsewhere in the world (Martin, 1994).

3.10. Mafic granulite (Gm)

Mafic granulite occurs interlayered with all kinds of gneisses, ranging in thickness from a few centimeters to a few meters (Plate 2A, B). In the western part the mafic granulite forms a relatively large mass of 700 x 200 m. The mafic granulite layers are sometimes oblique against the layers or foliation of the neighboring gneisses (Plate 6C), and the grain size of the mafic granulite is rarely observed gradually change from fine-grained near the contact with the garnet felsic gneiss to the coarse grains in the center of the layer. This indicates that a precursor of some mafic granulites is intrusive rock. In the southern part, irregular-shaped patches or pods or veins of the mafic granulite occur in the orthopyroxene felsic gneiss (Plate 3E).

Most mafic granulites are medium-grained and granoblastic-polygonal in texture (Plate 5D). There are at least two types of mafic granulite: one includes quartz and the other does not. The quartz-bearing type is light-gray, but the quartz-free variety is dark-gray in color. Also, the grain size tends to be finer in the quartz-bearing type than the quartz-free one. The observed mineral associations in the mafic granulite are as follows:

(1) clinopyroxene + plagioclase,
(2) clinopyroxene + plagioclase + quartz,
(3) clinopyroxene + orthopyroxene + plagioclase,
(4) orthopyroxene + quartz + plagioclase,
(5) clinopyroxene + orthopyroxene + quartz + plagioclase.

Apatite, ilmenite and magnetite are accessories. Small amounts of hornblende and/or biotite are rarely included as primary phases. Partial replacement of pyroxenes to actinolite or hornblende occurs.

Both the quartz-free and the quartz-bearing mafic granulites have basaltic compositions, with SiO_2 content ranging from 47 to 49 wt% and from 50 to 52 wt%, respectively. Both types are plotted in the non-alkaline field on the alkali-silica diagram, and exhibit a tholeiitic differentiation trend. The REE patterns are, however, different

between types, namely, the quartz-free type shows a relatively flat pattern in LREE as well as HREE with slightly positive Eu anomaly, while the quartz-bearing variety is enriched in LREE with relatively flat HREE and no Eu anomaly.

3.11. Anorthosite (A)

Anorthosite, having gray-black color, is restricted to the southwestern part and associated with mafic granulite, but the contact relationship between these rocks is obscure in the field. The anorthosite is massive and generally displays granular texture defined by coarse-grained calcic plagioclase with or without orthopyroxene, clinopyroxene and Fe-Ti oxide.

3.12. Ultramafic rocks (U)

Ultramafic rocks are distributed sporadically in the area, and several rock types such as clinopyroxenite, orthopyroxenite and peridotites are recognized. They commonly occur as lenticular or rounded blocks with diameters of a few tens of centimeters to several meters. The blocks of clinopyroxenite and peridotites are in clear contact with the host gneiss, while a pale blue quartz rind commonly surrounds the blocks of orthopyroxenite. In the southern part the peridotites occur as layers of several tens of centimeters thickness within the orthopyroxene felsic gneiss (Plate 3F); strongly foliated peridotites develop at the contact between the peridotites and orthopyroxene felsic gneiss.

The clinopyroxenite is black and massive, while the orthopyroxenite is yellow to pale brown and also massive. Clinopyroxene and orthopyroxene are the main constituent minerals in the clinopyroxenite and orthopyroxenite, respectively. The peridotites, which comprise mainly olivine, clinopyroxene and orthopyroxene (Plate 5E), are also yellow to pale brown in color, and commonly massive but rarely foliated as defined by elongated orthopyroxene. These main constituent minerals are generally coarse-grained and equigranular. Accessory minerals include biotite or phlogopite, spinel, magnetite, and rarely plagioclase.

The whole-rock compositions of the ultramafic rocks are different between the phlogopite-free and -bearing types. The SiO_2 content ranges from 43 to 48 wt% in the phlogopite-free type, and from 40 to 50 wt% in the phlogopite-bearing variety. The phlogopite-bearing type exhibits a variation trend in other oxides such as Al_2O_3, MgO and CaO against SiO_2, indicating an igneous differentiation trend similar to that of komatiitic rocks. The phlogopite-free type also shows a similar trend but more gently, its protolith is considered to be a depleted mantle peridotite. Very low REE concentrations ranging from 1 to 40 times chondrite values are characteristic of the ultramafic rocks. The phlogopite-bearing type exhibits the slightly LREE-enriched and flat HREE pattern, while the REE patterns of the phlogopite-free variety are rather flat in LREE as well as HREE.

4. Intrusive Rocks (M)

Abundant mafic dikes, which are generally referred to the Amundsen Dikes, occur in the ultra-high temperature metamorphic rocks throughout the area, striking N-S and NE-SW (Plate 6D). The widths of mafic dikes vary from several tens of centimeters to a few meters, but rarely reach 100 m. A chilled margin (several centimeters in thickness) is well developed at the contact with host metamorphic rocks, but thin mafic dikes lack a distinct chilled margin. No thermal effect is observed in the host gneiss. The Rb-Sr whole-rock data show 1190 ± 200 Ma for the intrusion age of the Amundsen Dikes (Sheraton and Black, 1981).

Most mafic dikes are black- to dark-gray-colored and massive, and display subophitic to intergranular textures. Light-gray-colored mafic dikes also occur; they are commonly porphyritic in texture. Relatively thick mafic dikes, being more than a few tens of meters thick, have coarse-grained and equigranular (gabbroic) texture in the central portion. Constituent minerals of igneous origin include clinopyroxene, plagioclase, magnetite and ilmenite with or without biotite and apatite (Plate 5F). Of these, two types of mineral associations can be recognized, namely, clinopyroxene + plagioclase + biotite ± apatite and clinopyroxene + plagioclase. Clinopyroxene in the biotite-bearing rocks exhibits pale-red to pale-green pleochroism. When the mafic dikes are porphyritic, the phenocrysts comprise plagioclase and clinopyroxene. Most commonly, plagioclase is chemically zoned. Although the mafic dikes are free of the Napier ultra-high temperature metamorphic episode, some of the mafic dikes are partially recrystallized to the following secondary mineral assemblages: 1) blue-green hornblende + meta-plagioclase, 2) blue-green hornblende + meta-biotite + meta-plagioclase, 3) blue-green hornblende + garnet + meta-plagioclase, 4) blue-green hornblende + meta-biotite + garnet + meta-clinopyroxene + meta-plagioclase, 5) blue-green hornblende + meta-biotite + garnet + meta-clinopyroxene + meta-plagioclase + orthopyroxene, 6) blue-green hornblende + meta-biotite + garnet + epidote + meta-plagioclase. Accessory secondary minerals include quartz, pyrite and chalcopyrite. These observations indicate that the mafic dikes were metamorphosed in the epidote-amphibolite to amphibolite facies conditions, probably related to the formation of the shear zone in the Riiser-Larsen area. Representative whole-rock XRF analyses are listed in Table 3. All of the analyzed samples are basaltic in SiO_2 content. The alkali-silica diagram shows that there are at least two types, alkaline and non-alkaline types. The biotite-bearing rocks belong to the alkaline type. The non-alkaline type shows a systematic increase in TiO_2 with increasing FeO*/MgO ratio, suggesting tholeiitic differentiation. The Nb-Zr relationships further subdivide the alkaline type into Type-A1 and -A2, and the non-alkaline type into Type-B1 and -B2. The Nb/Zr ratio is different between types-A1 and -A2, while Types-B1 and -B2 have similar Nb/Zr ratios but different abundances in Nb and Zr. Although the mafic dikes in the area exhibit similar modes of field occurrence, their petrography and petrochemistry indicate that they are diverse in lithology, and also diverse in origin.

Table 3. Whole-rock chemical analyses of mafic dikes (Amundsen Dikes) from Mount Riiser-Larsen.

Sample No.	HI96123 007	HI97010 401	HI97010 405	HI97021 101	HI97011 404	HI97012 208	HI97020 501	HI97020 701	HI97020 801	HI96122 903	HI96123 106	HI97011 606	HI97012 207	HI97010 604	HI97012 901	HI97020 802	HI97020 901
Dike Type	A1	A1	A1	A1	A2	B1	B1	B1	B1	B2	B2	B2	B2	B2	B2	B2	B2
SiO_2 (wt%)	44.86	44.48	44.78	45.24	48.39	55.19	54.94	51.78	51.63	50.72	51.03	49.22	49.77	50.73	50.29	49.46	49.58
TiO_2	3.24	3.16	3.23	3.33	3.22	1.57	1.52	1.89	2.08	1.53	0.85	1.54	0.85	1.18	0.69	1.37	1.66
Al_2O_3	14.70	14.55	14.84	14.70	12.24	11.16	10.66	12.61	12.43	12.84	15.14	12.86	15.42	12.94	15.77	13.16	14.07
Fe_2O_3	15.71	16.25	15.67	16.07	17.61	14.09	14.31	16.97	16.88	15.76	12.48	16.12	12.32	13.98	10.49	14.48	14.85
MnO	0.21	0.21	0.18	0.21	0.24	0.16	0.17	0.21	0.22	0.22	0.18	0.23	0.18	0.21	0.16	0.20	0.19
MgO	5.40	5.80	5.22	5.12	2.99	4.92	5.55	4.39	3.80	5.77	6.89	5.82	6.16	6.53	7.24	6.86	5.96
CaO	8.58	8.41	8.11	8.51	7.32	7.71	8.06	8.49	7.81	9.95	11.47	10.20	11.13	10.80	12.02	10.88	10.67
Na_2O	2.80	2.74	2.76	2.84	2.79	3.08	2.74	2.39	2.78	2.31	2.17	2.39	2.03	2.30	2.14	2.06	2.32
K_2O	1.80	1.72	1.85	1.91	2.82	1.44	1.33	1.22	1.46	0.65	0.44	0.46	0.41	0.51	0.34	0.16	0.20
P_2O_5	0.96	0.92	0.94	0.96	1.12	0.14	0.12	0.25	0.35	0.11	0.06	0.14	0.06	0.08	0.04	0.08	0.10
Total	98.25	98.21	97.57	98.86	98.74	99.44	99.39	100.18	99.42	99.87	100.70	98.97	98.33	99.25	99.17	98.71	99.60
(XRF)																	
Ba (ppm)	1242.6	1202.1	1181.1	1263.6	1036.4	326.2	300.7	430.3	532.7	172.5	173.1	171.5	198.4	131.3	121.3	37.1	24.4
Co	49.2	50.7	48.4	48.3	37.3	51.5	52.2	50.8	50.2	53.5	49.3	55.8	50.1	52.7	45.1	54.0	46.2
Cr	196.0	222.3	222.3	218.3	152.5	385.3	488.5	335.7	401.2	216.0	289.4	187.9	391.8	358.0	269.2	415.8	248.1
Cu	44.0	42.9	44.0	48.7	26.8	325.7	396.6	84.4	66.2	104.3	136.3	115.1	134.6	97.0	103.1	236.0	94.3
Nb	39.8	37.8	40.8	41.0	28.6	11.5	10.9	8.6	9.7	6.8	4.4	7.1	4.2	4.1	3.2	5.1	6.3
Ni	94.2	106.2	112.9	129.5	77.4	158.0	200.5	180.7	186.6	113.8	110.5	98.3	177.1	169.5	113.3	203.8	136.6
Rb	46.1	39.9	55.1	48.7	95.3	57.3	51.5	30.4	37.4	19.9	10.8	10.7	12.0	16.1	11.2	3.3	5.4
Sr	423.3	420.2	428.6	418.3	247.0	279.2	273.2	223.3	238.6	180.6	180.9	180.1	193.1	174.5	178.7	124.4	140.1
V	239.6	242.1	240.9	240.4	65.6	212.4	215.2	399.7	336.3	352.0	266.0	348.0	243.7	316.4	220.8	356.2	375.5
Y	29.5	28.9	29.8	32.0	68.9	26.3	24.5	38.4	44.1	31.1	22.2	32.9	22.4	23.3	17.1	26.4	26.5
Zn	122.2	125.2	111.9	120.2	162.6	133.7	114.7	132.5	144.1	120.4	86.5	115.3	87.9	98.1	71.6	97.6	106.5
Zr	157.1	147.5	161.8	163.7	291.0	173.4	166.3	160.3	194.5	114.8	64.9	105.8	67.4	83.8	52.1	81.4	94.7

All analytical data are after Ishizuka unpublished data.

5. Cenozoic Deposits

On the basis of the landforms and facies, Cenozoic deposits are classified into the following mapping units: glacial till, marine (m), talus (tl) and fluvial (f) deposits. The glacial tills are subdivided into two groups: older till (To) and younger till (Ty) on the basis of morphology and degree of weathering. Periglacial sediments and some talus deposits are omitted in this map because of their negligible amounts.

5.1. Older till (To)

The older till is a large quantity of glacial deposit forming large moraine fields in the area. The older till is thicker and its surface is more weathered than that of the younger till (Miura *et al.*, 1998b). Remarkable patterned grounds, mostly sorted polygons, sizes of which vary from 2 m to 5 m in diameter, and possible rock glaciers at the foot of the mountain are found on the surface of the moraine field (Hayashi, 1990; Saigusa *et al.*, 1998). The degree of weathering of the older till in a valley to the east of the peak (868 m), however, is slightly weaker than that in the other places. Probably it is due to delay of the ice sheet retreating to the north and the west in the valley (Miura *et al.*, 1998a). This older till in the valley is expressed by the symbol To' on the map. The older till is present mainly on the northern and western slopes on the lower parts of mountain flanks and glaciated valley walls; its surface is gentle or almost flat. It is poorly lithified and composed of subangular to subrounded rock fragments of cobble to boulder size with a matrix of pebble, granule, sand and silt. The gentle and undulating surface of the moraine field can be traced up to the north-facing slope of about 500 m asl. The older till and glacial erratics have not been found above about 500 m asl. Furthermore, the bedrock has no glacial polish or striations, and is commonly deeply weathered there (Hayashi, 1990; Zwartz *et al.*, 1998). The presence of a glacial trimline indicates that the level of the former ice sheet surface was at this height, at its maximum stage. Glacial striae running E-W on hill tops suggest that the ice sheet had once been flowing from east to west. This direction is accordant with that of Adams Fjord.

On the wall of a fluvial channel to the east of Richardson Lake, the older till is interstratified with a lacustrine deposit, "Richardson Clay" (Hayashi, 1990). Akiyama *et al.* (1990) have found the remains of protonematoid moss plants covered with diatom shells from the Richardson Clay and report that the diatom community is composed of at least 2 species of *Achnanthes* and 2 species of *Pinnularia*. Furthermore, Hayashi and Miura (1989) describe a large quantity of crystals of pyrite and vivianite in it which were produced by bacterial processes from phosphate-rich brackish water under anoxic reducing conditions. The Richardson Clay and thin coatings of calcite within the older till were dated by accelerator mass spectrometry (AMS) radiocarbon and thermoluminescence (TL) dating: the ages are 40,250 ± 1,200 ^{14}C yr BP for the clay and 42,570 ± 670 ^{14}C yr BP and ca. 71 ka (TL) for the calcite sample. Although these ages might be too young, due to contamination by younger carbon or other factors, the true age of crystallization of the calcite is not much older than the Last Interglacial stage at the oldest estimate from the provisional result of TL dating (Takada *et al.*, 1998). Additional age determinations for the older till, however, are urgently needed.

5.2. Younger till (Ty)

Several moraine ridges are found near the margin of the present ice sheet and/or local glaciers. These moraine ridges are formed from younger tills of thin loose unsorted fresh debris, mainly angular boulders and often ice cored. On the western coast, several moraine ridges with small and elongate ponds extend several hundred meters from northeast to southwest, parallel to the ice margin. The outer ice-marginal moraine surface is much more weathered than the inner ice-marginal moraine surface (Miura *et al.*, 1998a, b). These weathered moraine ridges suggest that the geohistory of the ice sheet has a small re-advanced or stagnant stage after the deposition of the older till. This till is expressed by a symbol Ty' on the map. The age of younger tills has not been revealed yet.

5.3. Marine deposits (m)

Several small raised beaches can be found up to 15 m asl in the southwestern part of this area (Zwartz *et al.*, 1998). Rounded boulders are widespread there and fine materials occur only near the present shoreline. Marine fossil shells for dating have not been found yet.

5.4. Talus deposits (tl)

Talus deposits by rock fall are present extensively at the foot of glaciated steep valley walls and at mafic dikes. The deposits consist of loose unsorted fresh angular boulders.

5.5. Fluvial deposits (f)

To the east of Richardson Lake, a remarkable meltwater channel and fluvial deposits are found in the valley extending for about 2 km from a small glacier. The gorge 5 to 15 m deep is incised into the older till. This is composed of subrounded to rounded cobble and boulders with matrix of pebbles, granules, sand and silt. In the upstream area, the channel, 3 to 5 m deep and about 50 m wide, is incised into the moraine field. At the mouth of the channel, a small delta is being formed with fine materials, mainly sand with granules. Fine fluvial deposits are found at the beach covered with snow drift in the southwestern part of this area.

6. Geologic Structures

The metamorphic rocks commonly show compositional layers (several millimeters to centimeters in thickness) which are generally parallel to lithological boundaries. The regional strikes are disturbed due to a large-scale dome (Plate 6A), and regional foliations generally dip to the east in the eastern area, the south in the central area, and the north in the western block. However, on an outcrop scale, foliations are locally folded by isoclinal folds. The majority of the metamorphic rocks have a granoblastic texture; however, some metamorphic rocks show mineral lineations defined by elongated quartz, sillimanite and orthopyroxene. Here we define the mineral lineations as L_n lineations. The trends of L_n mineral lineations are generally NNE-SSW, and they are generally

parallel to the compositional bands. Both the foliations and the mineral lineations were re-oriented by a late stage of doming. Details of the deformations are described below.

6.1. Folds

Field correlation shows at least two folding phases termed F_n and F_{n+1} in order of development. These folds suggest that metamorphic rocks of Mount Riiser-Larsen behaved as ductile materials at an early deformation stage. The geological cross section demonstrates the presence of outcrop-scale isoclinal overturned folds. We can also see isoclinal, overturned, recumbent folds of handspecimen-scale with subhorizontal fold axial planes (Plate 6B). The folds are termed F_n folds. The wavelength of F_n folds ranges up to one hundred of meters. Trends of fold axes are NNE-SSW, and are subparallel to those of L_n mineral. This suggests that F_n folding and formation of the L_n mineral lineation were nearly coeval under the granulite-facies conditions. However, the F_n folding ceased before peak ultra-high temperature metamorphism because the symplectic intergrowth of sapphirine and quartz are preserved.

Post-F_n folding is represented by a dome. The dome clearly disturbed the regional dips of lithological boundaries, compositional bands and axial surfaces of F_n folds. Therefore they generally dip 30°E to S, except in the western block where they dip to the north.

6.2. Boudinage

Garnet gneiss, characterized by higher strength than quartz-feldspar-rich gneisses, occurs as symmetrical boudinaged lenses at the bottom of the massive gneiss unit. The boudinization reflects the intense shear along the boundary between massive gneiss unit and layered gneiss unit.

6.3. Intrusion of mafic dikes

Mafic dikes, which are referred to the Amundsen Dikes, intruded into the whole Mount Riiser-Larsen area in the late Proterozoic (Plate 6D). They cut F_n isoclinal folds and post-F_n domes. These mafic dikes occur in two main sets: a N-S trending parallel set, and a NE-SW trending set. The emplacement of mafic dikes (1190 ± 200 Ma) apparently postdated the Napier metamorphic episode and predated the formation of the shear zones.

6.4. Mylonite and pseudotachylite

A large-scale N-S trending shear zone, which is referred to as the Riiser-Larsen Main Shear Zone (RLMSZ), is recognized in the western area. The RLMSZ separates the Mount Riiser-Larsen into the main and the western blocks. The main block is characterized by south dips of the foliation, the western block by north dips. In addition, there is a 1-2 kb pressure gap between the main and western structural units (Hokada, 1999). The RLMSZ and related N-S and NE-SW minor shear zones deformed the Amundsen Dikes and the host gneisses, and the related layer-parallel shear zones cut the Amundsen Dikes. The layer-parallel shear zones sometimes record a top-to-the north component of shear. The displacement is unknown. Near the shear zones, the gneisses and the mafic dikes are also sheared to mylonites or sometimes pseudotachylite-like rocks (Plate 6E, F). Mineral texture and mineral assemblage as described before indicate these

mafic dikes and gneisses to be free of the ultra-high temperature metamorphism of the Napier Complex. The formation of the shear zones apparently postdated the late Proterozoic mafic magmatism. It may be coeval with the Pan-African orogeny which is recognized in the Lützow-Holm Complex.

7. Geochronology

The geochronological data of whole-rocks and minerals from the Mount Riiser-Larsen area are summarized in Table 4. All data were obtained from samples collected by geology parties of the Japanese Antarctic Research Expedition. The ages are younger than 3.0 Ga and roughly show the two peaks of 2.7 to 3.0 Ga and 2.3 to 2.5 Ga. These peaks correspond to three tectonothermal events at 2.9 to 3.1 Ga (D1-M1: deformation stage 1 - metamorphic stage 1), 2.8 Ga (D2-M2) and 2.4 to 2.5 Ga (D3-M3) as demonstrated for the evolution of the Napier Complex (*e.g.* Sheraton *et al.*, 1987).

Sm-Nd whole-rock isochron ages were 3015 ± 44 Ma (initial Nd ratio (IR): 0.508554 ± 0.000026, MSWD: 0.00, εNd(T): -3.4 ~ -3.3) for orthopyroxene felsic gneiss, 2921 ± 186 Ma (IR: 0.508631 ± 0.000180, MSWD: 0.07, εNd(T): -4.4 ~ -4.1) for mafic granulite, and 2630 ± 143 Ma (IR: 0.508850 ± 0.000148, MSWD: 0.45, εNd(T): -8.3 ~ -6.9) for meta-ultramafic rocks. These isochron data may show the formation ages of their protoliths. The negative values of εNd(T) indicate these protoliths to be derived from enriched material (Suzuki, 2000). Sm-Nd mineral ages were obtained from garnet gneiss (2364 ± 22 Ma (IR: 0.509199 ± 0.000071, MSWD: 0.85)), garnet felsic gneiss (2382 ± 32 Ma (IR: 0.509065 ± 0.000223, MSWD: 22.05)), and mafic granulite (2380 ± 18 Ma (IR: 0.509448 ± 0.000022, MSWD: 0.02) and 2295 ± 129 Ma (IR: 0.509269 ± 0.000133, MSWD: 0.38)). These ages indicate that the final thermal event occurred at ca 2.4 Ga for Sm-Nd systematics (Suzuki, 2000).

Zircons from garnet felsic gneiss analyzed by Sensitive High Resolution Ion Microprobe (SHRIMP) at the Research School of Earth Sciences, the Australian National University, show two peaks of U-Pb isotopic ages at 2.4 to 2.6 Ga and 2.8 Ga. These two peaks are consistent with the Sm-Nd whole-rock and mineral isochron ages.

U-Th-Pb monazite and zircon chemical ages using EPMA (CHIME ages) have also been reported for quartzite, quartzo-feldspathic gneiss, garnet-orthopyroxene quartzo-feldspathic gneiss, garnet felsic gneiss and orthopyroxene felsic gneiss (Asami *et al.*, 1998; Hokada, 1999; Suzuki, 2000). Most of these ages range from 2.3 to 2.6 Ga. However, some zircon grains from sapphirine-orthopyroxene-bearing quartzo-feldspathic gneiss (TH97020713) and orthopyroxene felsic gneiss (SS97011304, SS97012402) remain the older ages of 2.7 to 2.9 Ga. In the sapphirine-osumilite-bearing layer in the garnet-orthopyroxene quartzo-feldspathic gneiss, the monazite and zircon grains embedded within osumilite yield ca 2.5 Ga (Hokada, 1999). This indicates that the monazite and zircon grains have been crystallized before or simultaneously with osumilite crystallization. Therefore, the timing of UHT metamorphism crystallizing osumilite may be ca 2.5 Ga, but not 2.8 Ga as interpreted by Harley and Black (1997).

Table 4. Ages of the metamorphic and igneous rocks from Mount Riiser-Larsen.

Method	Rock type	Age	Sample No.	ref.
Sm-Nd whole-rock isochron	orthopyroxene felsic gneiss	3015 ± 44 Ma (IR: 0.508554 ± 0.000026) (εNd(T): -3.4 ~ -3.3)	SS97011304 SS97011306 SS97012401	1
	mafic granulite (quartz-bearing type)	2921 ± 186 Ma (IR: 0.508631 ± 0.000180) (εNd(T): -4.4 ~ -4.1)	SS97013002 SS97020510 SS97021310	1
	meta-ultramafic rock	2630 ± 143 Ma (IR: 0.508850 ± 0.000148) (εNd(T): -8.3 ~ -6.9)	HI96123105D HI96123105L HI97010801 HI97010803U HI97010803F HI97010805 HI97012102 HI97012103	1
Sm-Nd mineral isochron	garnet felsic gneiss	2382 ± 35 Ma (IR: 0.509065 ± 0.000223)	SS97021307	1
	mafic granulite (quartz-free type)	2380 ± 18 Ma (IR: 0.509448 ± 0.000022)	SS97021303B	1
	mafic granulite (quartz-bearing type)	2295 ± 129 Ma (IR: 0.509269 ± 0.000133)	SS97021310	1
	garnet gneiss	2364 ± 22 Ma (IR: 0.509199 ± 0.000071)	SS97021208	1
U-Pb SHRIMP	garnet felsic gneiss	z: 2435 ± 27 ~ 2639 ± 57 Ma 2800 ± 32 ~ 2826 ± 21 Ma m: 2391 ± 59 ~ 2464 ± 40 Ma	SS97021307	1 1 1
U-Th-Pb CHIME (EPMA chemical dating)	orthopyroxene felsic gneiss	z: 2402 ± 32 ~ 2445 ± 82 Ma m: 2404 ± 54 Ma	MA88022102	2 2
		z: 2.4 ~ 2.6 Ga, 2.8 ~ 2.9 Ga	SS97011304 SS97012401	1
		z: 2.4 ~ 2.6 Ga	SS97012101	1
	garnet felsic gneiss	z: 2.3 ~ 2.5 Ga	SS97021307	1
		z: 2.3 ~ 2.5 Ga, m: 2.1 ~ 2.5 Ga	TH97012006	3
	quartzo-feldspathic gneiss	z: 2.4 ~ 2.6 Ga, 2.7 ~ 2.9 Ga	TH97020713	3
	quartzite (siliceous gneiss)	z: 2.4 ~ 2.6 Ga	TH97021326	3
		m: 2.4 ~ 2.5 Ga	TH97011305	3
	garnet-orthopyroxene quartzo-feldspathic gneiss	z: 2.3 ~ 2.6 Ga	R98022302C R98022301A TH97012909	3
		m: 2.5 ~ 2.6 Ga	R98022301B	3
	sapphirine-bearing layer in garnet-orthopyroxene quartzo-feldspathic gneiss	z: 2.3 ~ 2.6 Ga, m: 2.3 ~ 2.6 Ga	TH97020414 TH97020415 TH97020416	3
^{40}Ar-^{39}Ar	mafic dike	0.8 ~ 1.1 Ga		4
	sheared gneiss	1.0 ~ 2.0 Ga		4

z: zircon m: monazite

1: Suzuki (2000) 2: Asami *et al*. (1998) 3: Hokada (1999) 4: Takigami *et al*. (1998)

Takigami *et al.* (1998) reported ^{40}Ar-^{39}Ar ages of the sheared felsic gneisses in the Riiser-Larsen Main Shear Zone and of the mafic dikes. Their results show that the ages range from 1.0 to 2.0 Ga and from 0.8 to 1.1 Ga, respectively. Takigami *et al.* (1998) mentioned that the ages of 0.8 to 1.1 Ga for the mafic dikes are similar to those of the Amundsen Dikes (Sheraton and Black, 1981).

References

Akiyama, M., Hayashi, M., Matsumoto, G.I. and Miura, K. (1990): Plant remains and related substances in the past lacustrine sediments of the Mt Riiser-Larsen area, Enderby Land, East Antarctica. Proc. NIPR Symp. Polar Biol., **3**, 207-217.

Aniya, M. (1989): Landforms in the Mt Riiser-Larsen Area, Amundsen Bay, Enderby Land, East Antarctica. Transactions, Japanese Geomorphological Union, **10**, 195-208.

Asami, M., Suzuki, K., Grew, E. S. and Adachi, M. (1998): CHIME ages for granulites from the Napier Complex, East Antarctica. Polar Geosci., **11**, 172-199.

Black, L. P., Williams, I. S. and Compston, W. (1986): Four zircon ages from one rock: the history of a 3930 Ma-old granulite from Mount Sones, Enderby Land, Antarctica. Contrib. Mineral. Petrol., **94**, 427-437.

Crohn, P.W. (1959): A contributions to geology and glaciology of the western part of Australian Antarctic Territory. Aust. Bur. Miner. Resourc. Bull., **52**, 103 p.

Grikurov, G.E., Znachko-Yavorsky, G.A., Kanenov, E.N. and Ravich, M.G. (1976): Explanatory notes to the geological map of Antarctica (Scale 1:5000000). Research Institute of Arctic Geology, USSR Ministry of Geology, Leningrad.

Harley, S.L. and Black, L.P. (1997): A revised Archaean chronology for the Napier Complex, Enderby Land, from SHRIMP ion-microprobe studies. Antarct. Sci., **9**, 74-91.

Hayashi, M. (1990): Glacial history with special reference to the past lacustrine deposits in the Mount Riiser-Larsen area, Enderby Land, East Antarctica. Proc. NIPR Symp. Antarct. Geosci., **4**, 119-134.

Hayashi, M. and Miura, K. (1989): Some notes on several characteristic minerals sampled from East Antarctica. Mem. Fac. Educa., Shimane Univ., Nat. Sci., **23**, 1-24.

Hokada, T. (1999): Thermal evolution of the ultrahigh-temperature metamorphic rocks in the Archaean Napier Complex, East Antarctica. Ph.D. Thesis, The Graduate University for Advanced Studies, 126p.

Hokada, T., Osanai, Y., Toyoshima, T., Owada, M., Tsunogae, T. and Crowe, W. A. (1999): Petrology and metamorphism of sapphirine-bearing aluminous gneisses from Tonagh Island in the Napier Complex, East Antarctica. Polar Geosci., **12**, 49-70.

Ishikawa, M., Motoyoshi, Y. and Fraser, G. L. (1994): Preliminary report of structures of Forefinger Point, Enderby Land, East Antarctica. Proc. NIPR Symp. Antarct. Geosci., **7**, 90-100.

Ishizuka, H., Ishikawa, M., Hokada, T. and Suzuki, S.(1998): Geology of Mount Riiser-Larsen of the Napier Complex, Enderby Land, East Antarctica. Polar Geosci., **11**, 154-171.

Kamenev, E. N. (1972): Geological structure of Enderby Land. Antarctic geology and geophysics, ed. by R.J. Adie. Oslo, Universitetsforlaget, 579-583.

Kamenev, E. N. (1975): The geology of Enderby Land. Acad. Sci. USSR Comm. Antarct. Res. Rept, 14.

Makimoto, H., Asami, M. and Grew, E. S. (1989): Some geological observations on the Archean Napier Complex at Mount Riiser-Larsen, Amundsen Bay, Enderby Land. Proc. NIPR Symp. Antarct. Geosci., **3**, 128-141.

Martin, H. (1994): Archaean grey gneisses and the genesis of continental crust. Archaean Crustal Evolution, ed. by K.C. Condie. Amsterdam, Elsevier, 205-259.

Mawson, D.(1932): The B.A.N.Z. Antarctic Research Expedition 1929-31. Geogr. J., **80**, 101-113.

McLeod, I.R. (1959): Report on geological and glaciological work by the 1958 Australian National Antarctic Research Expedition. Bureau of Mineral and Resources, Australia, Record 1959/131.

McLeod, I.R. (1964): An outline of geology of the sector from longitude 45° to 80°E., Antarctica. Antarctic Geology, ed. by R.J. Adie. Amsterdam, North-Holland Publ. Co., 237-247.

McLeod, I.R., Trail, D.S., Cook, P.J. and Wallis, G.R. (1966): Geological work in Antarctica, January to March, 1965. Bureau of Mineral and Resources, Australia, Record 1966/9.

Miura, H., Takada, M., Zwartz, D. P. and Moriwaki, K. (1998a): Weathering evaluation of glacial sediments at Mt Riiser-Larsen and its significance. The 17th NIPR Symposium on Antarctic Geosciences - Abstracts, 38-40.

Miura, H., Takada, M., Zwartz, D. P. and Moriwaki, K. (1998b): Preliminary report of East Antarctic ice sheet history on the basis of glacial landforms and sediments at Mt Riiser-Larsen. The 17th NIPR Symposium on Antarctic Geosciences - Abstracts, 41-43.

Motoyoshi, Y. (1996): Pseudotachylite from McIntyre Island, Enderby Land, East Antarctica: evidence for a rapid crystallization. Proc. NIPR Symp. Antarct. Geosci., **9**, 65-75.

Motoyoshi, Y. and Hensen, B. J. (1989): Sapphirine-quartz-orthopyroxene symplectites after cordierite in the Archaean Napier Complex, Antarctica: evidence for a counterclockwise *P-T* path? Eur. J. Mineral., **1**, 467-471.

Motoyoshi, Y. and Matsueda, H. (1984): Archean granulites from Mount Riiser-Larsen in Enderby Land, East Antarctica. Mem. Natl Inst. Polar Res., Spec. Issue, **33**, 103-125.

Motoyoshi, Y. and Matsueda, H. (1987): Corundum + quartz association in Archean granulite-facies rock from Enderby Land, East Antarctica: preliminary interpretation. Proc. NIPR Symp. Antarct. Geosci., **1**, 107-112.

Motoyoshi, Y., Hensen, B. J. and Matsueda, H. (1990): Metastable growth of corundum adjacent to quartz in a spinel-bearing quartzite from the Archaean Napier Complex, Antarctica. J. Metamorph. Geol., **8**, 125-130.

Motoyoshi, Y., Ishikawa, M. and Fraser, G. L. (1994): Reaction textures in granulites from Forefinger Point, Enderby Land, East Antarctica: an alternative interpretation on the metamorphic evolution of the Rayner Complex. Proc. NIPR Symp. Antarct. Geosci., **7**, 101-114.

Motoyoshi, Y., Ishikawa, M. and Fraser, G. L. (1995): Sapphirine-bearing silica-undersaturated granulites from Forefinger Point, Enderby Land, East Antarctica: evidence for a clockwise *P-T* path? Proc. NIPR Symp. Antarct. Geosci., **8**, 121-129.

Osanai, Y., Toyoshima, T., Owada, M., Tsunogae, T., Hokada, T. and Crowe, W. A. (1999): Geology of ultrahigh-temperature metamorphic rocks from Tonagh Island in the Napier Complex, East Antarctica. Polar Geosci., **12**, 1-28.

Owada, M., Osanai, Y. and Kagami, H. (1994): Isotopic equilibration age of Sm-Nd whole-rock system in the Napier Complex (Tonagh Island), East Antarctica. Proc. NIPR Symp. Antarct. Geosci., **7**, 122-132.

Owada, M., Osanai, Y., Toyoshima, T., Tsunogae, T., Hokada, T. and Crowe, W. A. (1999): Petrography and geochemistry of mafic and ultramafic rocks from Tonagh Island in the Napier Complex, East Antarctica. Polar Geosci., **12**, 87-100.

Rucker, R. A. (1963): Geological reconnaissance in Enderby Land and southern Prince Charles Mountains, Antarctica. Bureau of Mineral and Resources, Australia, Record 1963/154.

Saigusa, S., Miura, H., Maemoku , H. and Hirakawa, K. (1998): Preliminary reports of rock glaciers at the foot of Mount Riiser-Larsen in Enderby Land, East Antarctica. Nankyoku Shiryô (Antarct. Rec.), **42**, 168-178.

Sheraton, J. W. and Black, L. P. (1981): Geochemistry and geochronology of Proterozoic tholeiite dikes of East Antarctica: evidence for mantle metasomatism. Contrib. Mineral. Petrol., **78**, 305-317.

Sheraton, J. W., Tingey, R. J., Black, L. P., Offe, L. A. and Ellis, D. J. (1987): Geology of Enderby Land and Western Kemp Land, Antarctica. Aust. Bur. Miner. Resourc. Bull., **223**, 51 p.

Suzuki, S. (2000): Geochemistry and geochronology of ultra-high temperature metamorphic rocks from the Mount Riiser-Larsen area in the Archaean Napier Complex, East Antarctica. Ph.D. Thesis, The Graduate University for Advanced Studies, in press.

Suzuki, S., Hokada, T., Ishikawa, M. and Ishizuka, H. (1999): Geochemical study of granulites from Mount Riiser-Larsen, Enderby Land, East Antarctica: Implication for protoliths of the Archaean Napier Complex. Polar Geosci., **12**, 101-125.

Tainosho, Y., Kagami, H., Takahashi, Y., Iizumi, S., Osanai, Y. and Tsuchiya, N. (1994): Preliminary result for the Sm-Nd whole-rock age of the metamorphic rocks from Mount Pardoe in the Napier Complex, East Antarctica. Proc. NIPR Symp. Antarct. Geosci., **7**, 115-121.

Tainosho, Y., Kagami, H., Hamamoto, T. and Takahashi, Y. (1997): Preliminary result for the Nd and Sr isotope characteristics of the Archaean gneisses from Mount Pardoe, Napier Complex, East Antarctica. Proc. NIPR Symp. Antarct. Geosci., **10**, 92-101.

Takada, M., Miura, H. and Zwartz, D.P. (1998): Radiocarbon and thermoluminescence ages in the Mount Riiser-Larsen area, Enderby Land, East Antarctica. Polar Geosci., **11**, 239-248.

Takigami, Y., Ishikawa, N. and Funaki, M. (1998): Preliminary 40Ar-39Ar analyses of igneous and metamorphic rocks from the Napier Complex. Polar Geosci., **11**, 200-207.

Toyoshima, T., Osanai, Y., Owada, M., Tsunogae, T., Hokada, T. and Crowe, W. A. (1999): Deformation of ultrahigh-temperature metamorphic rocks from Tonagh Island in the Napier Complex, East Antarctica. Polar Geosci., **12**, 29-48.

Tsunogae, T., Osanai, Y., Toyoshima, T., Owada, M., Hokada, T. and Crowe, W. A. (1999): Metamorphic reactions and preliminary *P-T* estimates of ultrahigh-temperature metamorphic rocks from Tonagh Island in the Napier Complex, East Antarctica. Polar Geosci., **12**, 71-86.

Yoshida, Y. and Moriwaki, K. (1983): Landform of Mt Riiser-Larsen, Amundsen Bay, Enderby Land: results of a preliminary survey. Proc. NIPR Symp. Antarct. Geosci., **3**, 240-246.

Zwartz, D.P., Miura, H., Takada, M. and Moriwaki, K. (1998): Holocene lake sediments and sea-level change at Mt. Riiser-Larsen. Polar Geosci., **11**, 249-259.

Plate 1. *A: Easternmost ridge of Mount Riiser-Larsen. Massive gneiss unit composed mainly of orthopyroxene felsic gneiss with minor amount of mafic granulite (upper half) overlies layered gneiss unit which consists mainly of paragneisses with small amounts of felsic orthogneisses and mafic granulites (lower half). B: Peak of Mount Riiser-Larsen. View from north. Basement rocks crop out over the steep ridge, and extensive moraine field is developed on the lower part of mountain flanks.*

Plate 2

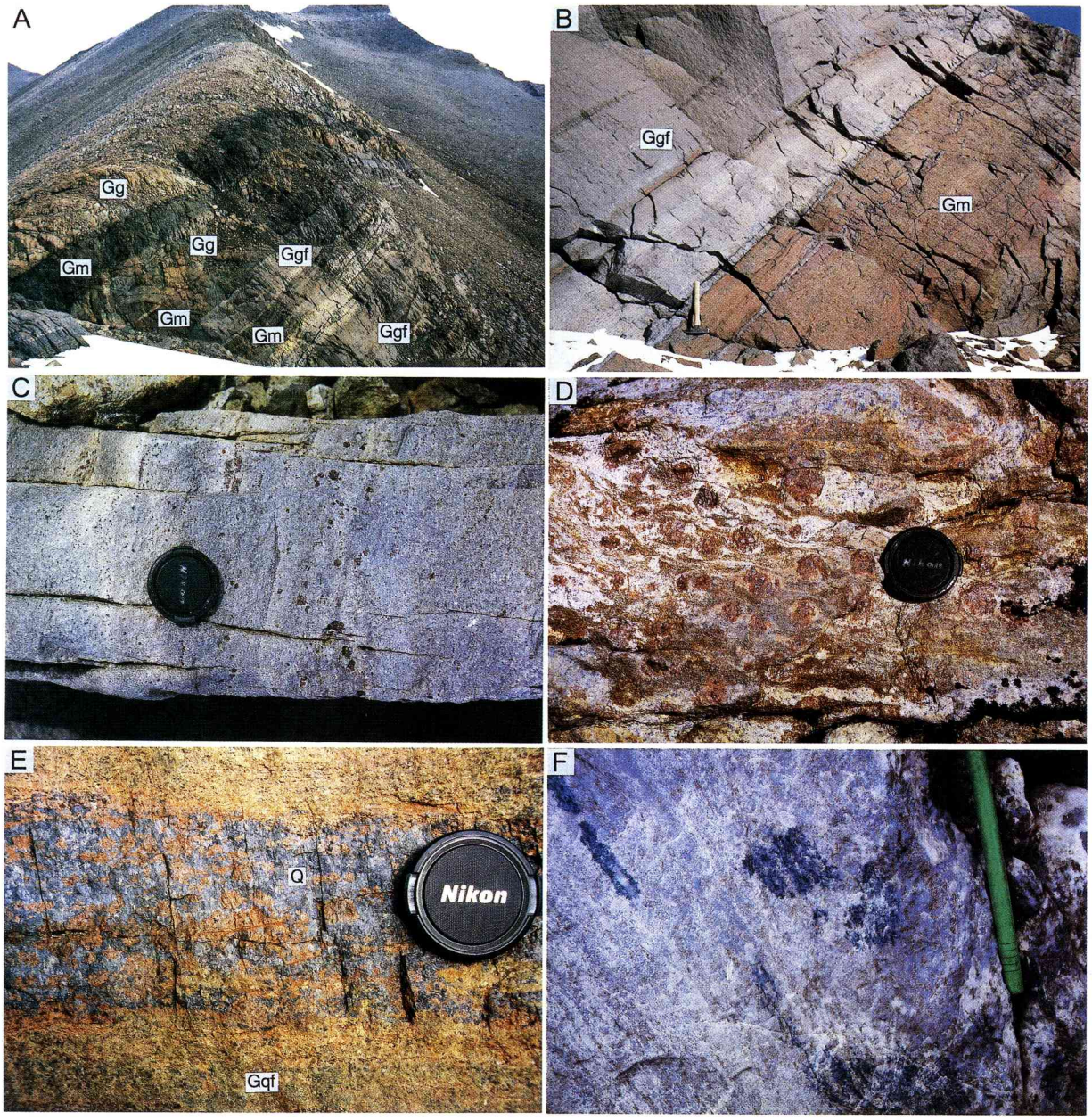

Plate 2. A: Well-layered structure composed of garnet gneiss (orange), garnet felsic gneiss (grayish pink) and mafic granulite (dark brown & reddish brown). The width of the photograph is approximately 40 m. B: Close up view of layering structure as shown in Plate 2A. Garnet felsic gneiss (grayish pink) and mafic granulite (reddish brown). C: Garnet felsic gneiss. D: Garnet-sillimanite gneiss. E: Quartzo-feldspathic gneiss (orange) and interleaved impure quartzite layer (blue). F: Sapphirine-bearing siliceous gneiss. Sapphirine-quartz-bearing irregular shaped patches occur in the gneiss.

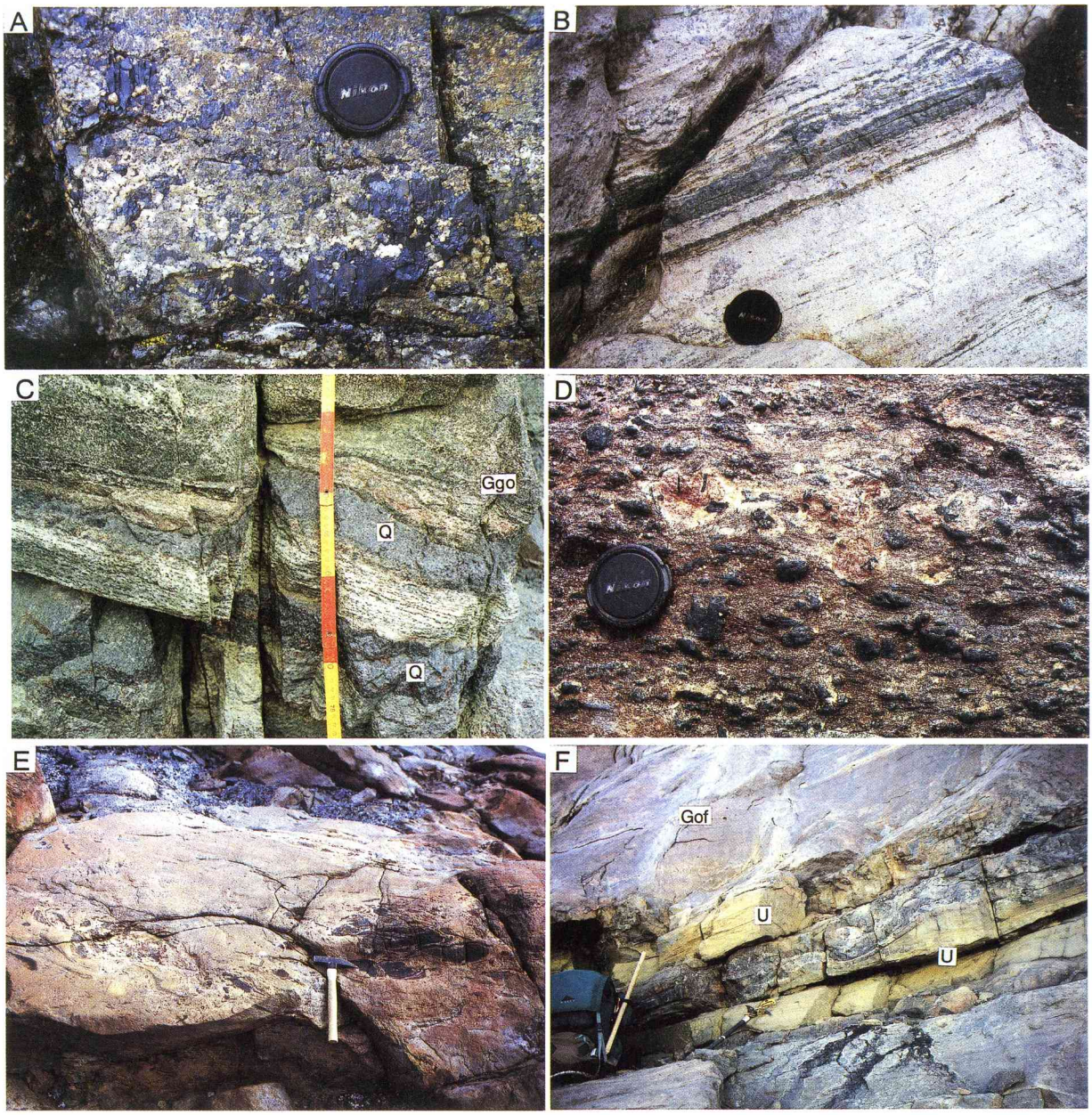

Plate 3. A: Magnetite-quartz gneiss. Magnetite porphyroblasts (black) occur in quartz and pyroxene rich portion (yellow). B: Sapphirine-bearing quartzo-feldspathic gneiss. Quartzo-feldspathic layers (white) and sapphirine-quartz-bearing thin layers (blue) constitute the gneiss. C: Layered structure of garnet-orthopyroxene quartzo-feldspathic gneiss. Impure quartzite layers (blue) are intercalated within the gneiss. D: Sapphirine-phlogopite gneiss. Coarse-grained and euhedral to subhedral sapphirine occurs in the phlogopite-rich matrix. Garnet is rarely present and surrounds sapphirine. E: Orthopyroxene felsic gneiss containing irregular-shaped patches of mafic granulite. F: Meta-ultramafic rocks occurring as sheet-like layers in orthopyroxene felsic gneiss.

Plate 4

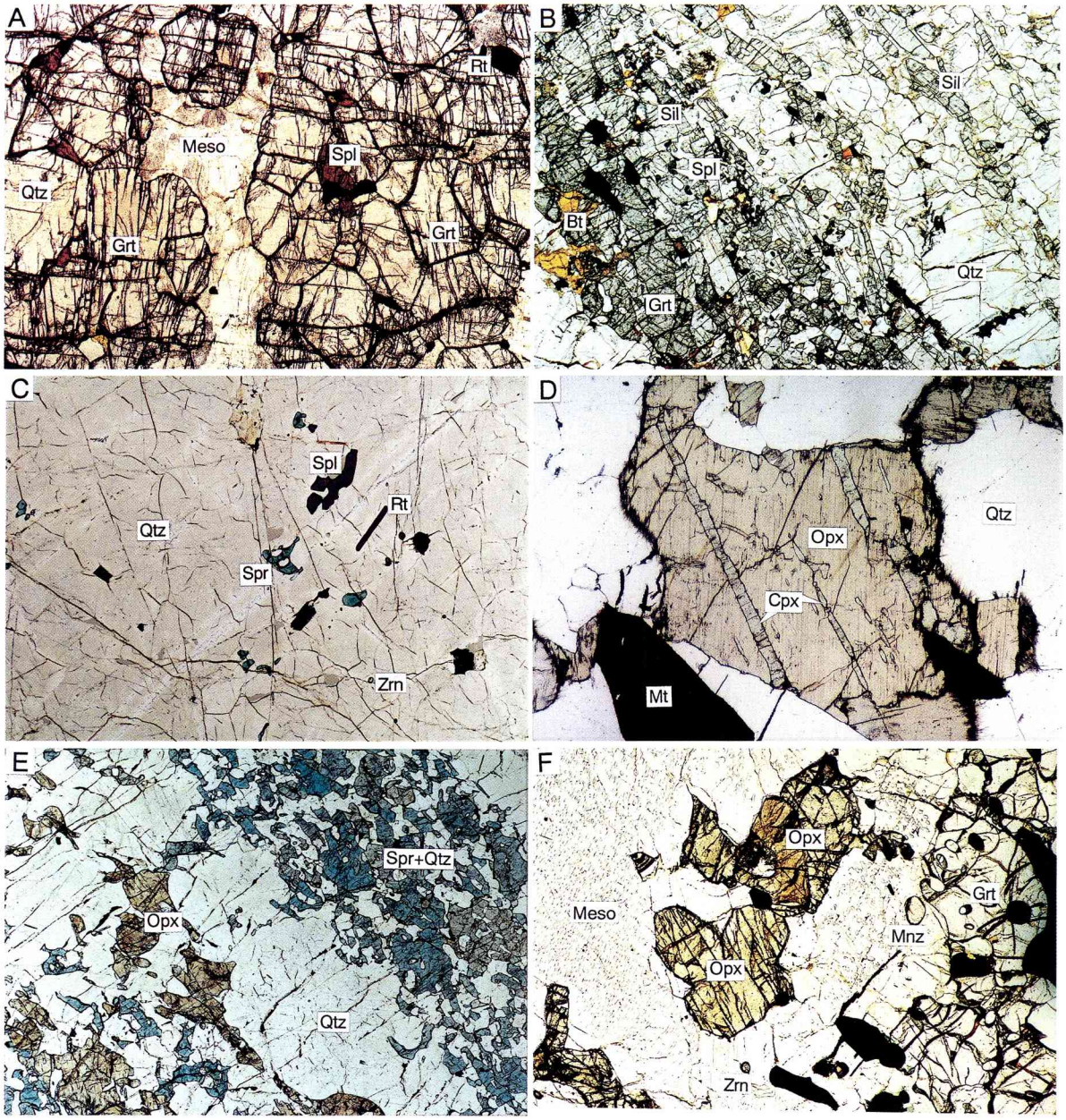

Plate 4. Photomicrograph of metamorphic rocks. Plane polarized light. A: Garnet gneiss (width = 6 mm). B: Garnet-sillimanite gneiss (width = 1.2 cm). C: Impure quartzite (width = 6 mm). D: Magnetite-quartz gneiss (width = 2 mm). Other than thick clinopyroxene lamellae (labeled 'Cpx' in photograph), fine clinopyroxene lamellae are also contained in orthopyroxene. E: Sapphirine-bearing quartzo-feldspathic gneiss (width = 6 mm). Sapphirine grains are associated with quartz. F: Garnet-orthopyroxene quartzo-feldspathic gneiss (width = 3 mm).

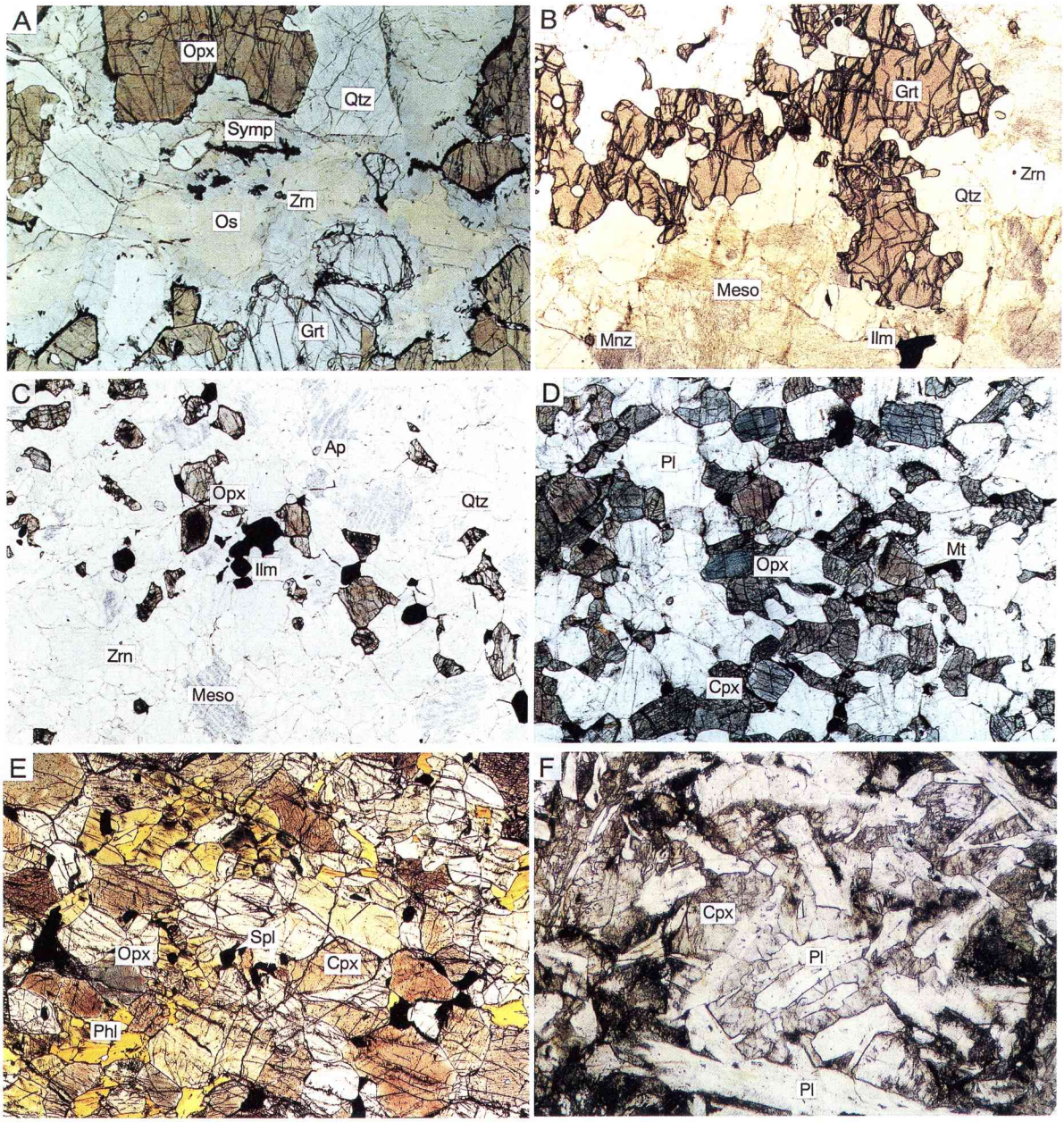

Plate 5. Photomicrograph of metamorphic and igneous rocks. Plane polarized light. A: Osumilite-bearing garnet-orthopyroxene quartzo-feldspathic gneiss (width = 3 mm). Osumilite is commonly replaced by fine-grained symplectites (labeled 'Symp') of cordierite-K-feldspar-quartz-orthopyroxene. B: Garnet felsic gneiss (width = 6 mm). C: Orthopyroxene felsic gneiss (width = 6 mm). D: Mafic granulite (width = 6 mm). E: Meta-ultramafic rock (width = 4 mm). F: Mafic dike (Amundsen Dikes) (width = 2 mm).

Plate 6

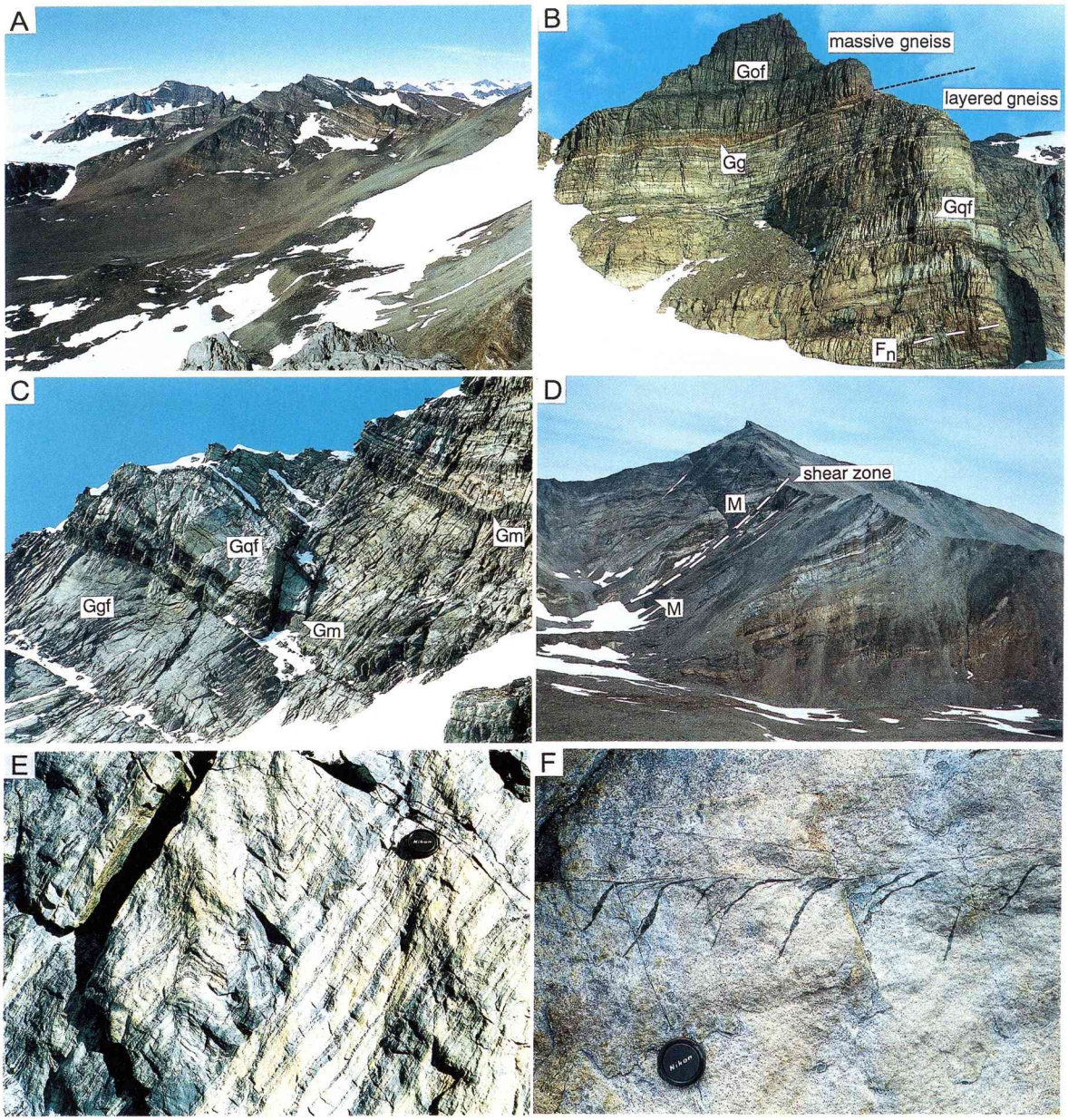

Plate 6. A: Dome structure on Mount Riiser-Larsen. B: An F_n isoclinal fold, which developed in the layered gneisses. The wavelength is about 50 m. C: Mafic granulites are slightly oblique to other kinds of gneisses. This suggests that the mafic granulites were mafic dikes in origin. D: Mafic dike, which was cut by the layer-parallel shear zone. E: Mylonite and related drag folds. F: Pseudotachylite, which occurs as en-echelon veins in the orthopyroxene felsic gneiss.

Antarctic Geological Map Series

Sheet 1	East Ongul Island 1:5,000	March 1974
Sheet 2	West Ongul Island 1:5,000	March 1974
Sheet 3	Teöya 1:5,000	March 1975
Sheet 4	Ongulkalven Island 1:5,000	March 1975
Sheet 5	Langhovde 1:25,000	March 1976
Sheet 6 & 7	Skarvsnes 1:25,000	March 1977
Sheet 8	Kjuka and Telen 1:25,000	March 1979
Sheet 9	Skallen 1:25,000	March 1976
Sheet 10	Padda Island 1:25,000	March 1977
Sheet 11	Cape Hinode 1:25,000	March 1978
Sheet 12	Lützow-Holm Bay 1:250,000	March 1989
Sheet 13	Prince Olav Coast 1:250,000	March 1989
Sheet 14	Sinnan Rocks 1:25,000	March 1983
Sheet 15	Cape Ryûgû 1:25,000	March 1980
Sheet 16	Akebono Rock 1:25,000	March 1986
Sheet 17	Niban Rock 1:25,000	March 1983
Sheet 18	Kasumi Rock 1:25,000	March 1984
Sheet 19	Tenmondai Rock 1:25,000	March 1985
Sheet 20	Akarui Point and Naga-iwa Rock 1:25,000	March 1984
Sheet 21	Cape Omega 1:25,000	March 1979
Sheet 22	Oku-iwa Rock 1:25,000	March 1981
Sheet 23	Honnör Oku-iwa Rock 1:25,000	March 1987
Sheet 24	Rundvågskollane and Rundvågshetta 1:25,000	March 1986
Sheet 25	Botnneset 1:25,000	March 1987
Sheet 26	Strandnibba 1:25,000	March 1985
Sheet 27 (1)	Mt. Fukushima, Northern Yamato Mountains 1:25,000	March 1978
Sheet 27 (2)	Mt. Torimai, Northern Yamato Mountains 1:25,000	March 1995
Sheet 28	Central Yamato Mountains, Massif B and Massif C 1:25,000	March 1982
Sheet 29	Belgica Mountains 1:25,000	March 1981
Sheet 30	Southern Yamato Mountains (Massif A and JARE-IV) 1:25,000	March 1988
Sheet 31	Balchenfjella 1:100,000	March 1991
Sheet 32	Widerøefjellet 1:100,000	March 1992
Sheet 33	Bergersenfjella 1:100,000	March 1993
Sheet 34	Brattnipene 1:100,000	March 1996
Sheet 35	Sør Rondane Mountains 1:250,000	March 1997
Sheet 36	Ongul Islands 1:10,000	March 1994
Sheet 37	Mount Riiser-Larsen 1:12,500	March 2000